

APPENDIX F

**REVISIONS TO REPORT ON DRIFT-SCALE COUPLED PROCESSES
(DRIFT SCALE TEST AND THERMAL-HYDROLOGIC-CHEMICAL SEEPAGE)
(RESPONSE TO ENFE 1.03 AIN-1)**

Note Regarding the Status of Supporting Technical Information

This document was prepared using the most current information available at the time of its development. This Technical Basis Document and its appendices providing Key Technical Issue Agreement responses that were prepared using preliminary or draft information reflect the status of the Yucca Mountain Project's scientific and design bases at the time of submittal. In some cases this involved the use of draft Analysis and Model Reports (AMRs) and other draft references whose contents may change with time. Information that evolves through subsequent revisions of the AMRs and other references will be reflected in the License Application (LA) as the approved analyses of record at the time of LA submittal. Consequently, the Project will not routinely update either this Technical Basis Document or its Key Technical Issue Agreement appendices to reflect changes in the supporting references prior to submittal of the LA.

APPENDIX F

REVISIONS TO REPORT ON DRIFT-SCALE COUPLED PROCESSES (DRIFT SCALE TEST AND THERMAL-HYDROLOGIC-CHEMICAL SEEPAGE) (RESPONSE TO ENFE 1.03 AIN-1)

This appendix provides a response for Key Technical Issue (KTI) agreement Evolution of Near-Field Environment (ENFE) 1.03 Additional Information Needed (AIN)-1. This agreement relates to providing additional information regarding simulation results for the drift-scale coupled thermal-hydrologic-chemical (THC) processes of the Drift Scale Test (DST) seepage in the drift-scale coupled THC processes model and documentation of model validation.

F.1 KEY TECHNICAL ISSUE AGREEMENT

F.1.1 ENFE 1.03 AIN-1

Agreement ENFE 1.03 was reached during the U.S. Nuclear Regulatory Commission (NRC)/U.S. Department of Energy (DOE) Technical Exchange and Management Meeting on Evolution of the Near-Field Environment (Reamer 2001) January 9 to 12, 2001, in Pleasanton, California. ENFE Subissues 1, 2, 3, and 4 were discussed at that meeting. ENFE 1.03 was discussed under Subissue 1, Effects of Coupled Thermal-Hydrologic-Chemical Processes on Seepage and Flow.

The wording of the agreement is as follows:

ENFE 1.03

Provide the Drift-Scale Coupled Processes (DST and THC Seepage) Models AMR, Rev. 01 and 02, including (1) information on the quantity of unreacted solute mass that is trapped in dry-out zone in TOUGHREACT simulations, as well as how this would affect precipitation and the resulting change in hydrologic properties and (2) documentation of model validation consistent with the DOE QA requirements. The DOE will provide documentation of model validation, consistent with the DOE QA requirements, in the *Drift-Scale Coupled Processes (DST and THC Seepage) Models* AMR (MDL-NBS-HS-000001) Rev 01, expected to be available to the NRC in March 2001. The DOE will provide information on the quantity of unreacted solute mass that is trapped in the dryout zone in TOUGHREACT simulations in the *Drift-Scale Coupled Processes (DST and THC Seepage) Models* AMR Rev 02, expected to be available to the NRC in FY 02.

The DOE response to this KTI agreement was provided in *Drift-Scale Coupled Processes (DST and THC Seepage) Models* (CRWMS M&O 2001), as specified in the agreement. After reviewing this report, the NRC determined that additional information was needed to complete KTI agreement ENFE 1.03. The results of the NRC review were stated as follows in a letter from NRC to DOE (Schlueter 2002):

Wording of the AIN is as follows:

ENFE 1.03 AIN-1

NRC Review: The NRC reviewed Drift-Scale Coupled Processes (DST and THC Seepage) Models (MDL-NBS-HS-000001, Rev 01, ICN 00) as it pertains to this agreement and it only partially satisfies the agreement. According to information received at the ENFE Technical Exchange (presentation by Sonnenthal and Apps, January 2001) this revision of the document was to contain the technical basis for neglecting coupled thermal-hydrological-chemical alterations of the Calico Hills nonwelded (CHn) hydrogeological units. Specifically, NRC was told MDL-NBS-HS-000001, Rev. 01, was to contain simulation results demonstrating that “resulting porosity, permeability, and mineralogical changes in the CHn are expected to be inconsequential.” Staff understands that the THC modeling described in MDL-NBS-HS-000001, Rev. 01, does include the CHn hydrogeological units, but simulation results specifically related to alteration of the CHn hydrogeological units are not presented in MDL-NBS-HS-000001, Rev. 01.

Additional Information Needed: In the next revision of the document, provide the information discussed above, as well as the information discussed in the second half of the agreement.

F.1.2 Related Key Technical Issue Agreements

Agreements ENFE 1.05 and ENFE 2.17 are related to agreement ENFE 1.03 in that both deal with the drift-scale coupled processes model. KTI agreements ENFE 1.07, ENFE 2.18, and ENFE 4.02 are concerned with providing a revision to the report documenting the drift-scale coupled processes model to the NRC and are to be addressed in separate documents.

F.2 RELEVANCE TO REPOSITORY PERFORMANCE

THC processes at the drift scale play an important part in the assessment of total system performance, as the simulations provide inputs for the drift chemical environments for waste package corrosion and degradation. The agreement is relevant to the repository performance, because the abstraction of THC seepage and the associated parameter values are directly used in total system performance assessment (TSPA) calculations and in the evaluation of the unsaturated zone.

F.3 RESPONSE

KTI Agreement ENFE 1.03 AIN-1 relates to documentation in Revisions 1 and 2 of the report on drift-scale coupled-process models (BSC 2002a; BSC 2003a) for the following three issues:

1. The treatment of unreacted solute mass trapped in the dryout zone in TOUGHREACT simulations and its impact on THC-induced hydrologic property changes.
2. Model validations consistent with the DOE quality assurance requirements.

3. Simulation results related to THC-induced alterations in the CHn unit.

The repository drift-scale THC seepage model is used in support of the TSPA in-drift geochemical model. Major revisions in Revision 2 of *Drift-Scale Coupled Processes (DST and THC Seepage) Models* (BSC 2003a, Section 1.1) include new simulations that make use of improved treatment of various modeled processes, updated hydrologic and thermal properties, and uncertainty in parameter quantification. Specifically, parameter uncertainty is quantified through considering five input water compositions (BSC 2003a, Section 6.2.2.1), some variations in infiltration rates, CO₂ effective diffusivity (two values), and the effect of vapor-pressure lowering caused by capillary pressure (BSC 2003a, Sections 6.4.6.1, Approximations 12 and 15, 6.8.5.2, and 6.8.5.3).

The model validation of Revision 2 of *Drift-Scale Coupled Processes (DST and THC Seepage) Models* (BSC 2003a) includes an in situ heater test (the Drift Scale Test), a plug-flow reactor experiment, and a fracture sealing experiment (BSC 2002a).

The response to this KTI agreement is divided into three parts, keyed to the three main issues of ENFE 1.03 AIN-1. Section F.3.1 presents the analyses of unreacted-solute precipitation, mineral alteration, porosity, and permeability changes. Section F.3.2 describes the THC model validation. Section F.3.3 provides the response to the comment regarding thermal alteration of the CHn unit.

The technical basis for the response (Section F.3) is provided in Section F.4. Specifically, Section F.4.1 describes the THC model, Section F.4.2 discusses the THC simulations and results, Section F.4.3 analyzes the effect of unreacted solutes and mineral precipitation on changes in porosity and permeability, Section F.4.4 describes model validation, and Section F.4.5 deals with the thermal alteration of the CHn unit.

F.3.1 Mineral Precipitation and Alteration and Accompanying Changes to Porosity and Permeability

Under continuous thermal loading from the radioactive decay of waste in the drift, moisture is driven away by the heat source, resulting in the formation of a dryout zone, where liquid saturation in the fracture or rock matrix is zero. In the fractured tuffs around the drift wall, pore water vaporizes and boils because of heating from the waste, and vapor migrates out of the matrix into fractures. The vapor subsequently moves away from the drift through the fracture network as vapor pressure increases. As a result, water content in the rock around the drift wall decreases. A dryout zone may develop at places close to the heat source under these conditions. With the boiling phase lasting about 1,000 years following waste emplacement, the associated dryout zone in the fractures around the drift is maximized at about 600 years and reaches approximately 12 m below the drift, 9 m to the side, and 8 m above the drift center (BSC 2003a, Figures 6.5-4, 6.7-4). In contrast, when the vapor reaches cooler regions (just below boiling) farther from the drift, it condenses on fracture walls and drains through the fracture network. The condensation water in fractures drains back to the edge of the fracture dryout zone, reflecting an equilibrium state between boiling and condensation processes. The condensed water slowly imbibes from fractures into the matrix, gradually leading to increases in the liquid saturation of the matrix. Related physical and chemical processes lead to increases in many

solute concentrations in the boiling zone and primarily mineral dissolution and reaction in the condensation zone. These alterations modify the porosity and permeability of the fractured rock.

F.3.1.1 Evaporitic and Mineral Precipitation at the Boiling–Evaporation Front

Solutes may accumulate and minerals may precipitate because of evaporation and boiling in the dryout and boiling zones. Under evaporation or boiling conditions, water evaporates into air to form water vapor. However, some unreacted solutes are concentrated in the remaining waters. These solutes will precipitate as minerals and accumulate in the dryout zone. Water that rewets the dryout zone following the thermal pulse will dissolve the precipitated chloride and nitrate salts, resulting in increased aqueous concentrations and consequent increase in pore-water ionic strength. These processes and corresponding effects have been captured in Revision 2 of *Drift-Scale Coupled Processes (DST and THC Seepage) Models* (BSC 2003a, Section 6.4.5) using TOUGHREACT V2.4 and V3.0. The quantity of the unreacted solutes was accounted for in Revision 2. For the major mineral phases and salts, results from the Revision 2 simulations show a greater abundance of precipitated minerals than those from Revision 1. As an example of the change in modeled mineral abundances, there was a maximum of about a factor of 3 increase in the calcite abundance in simulations of the Drift Scale Test using TOUGHREACT V3.0 (BSC 2003a, Figure 7.1-37) compared to TOUGHREACT V2.3 (BSC 2003a, Figure 7.1-35).

To account for the unreacted solutes in the dryout zone requires special treatment to overcome a potential mass-balance problem in simulations. The problem is related to the calculation of the quantity of a solute mass, which requires knowing both the concentration and associated water volume. However, the water content is reduced to zero following a dryout event. Consequently, precipitated minerals may not be accounted for in the mass-balance calculation because of the absence of water in the dryout gridblock. A method was developed for storing the residual aqueous species in a solid mineral assemblage in TOUGHREACT V2.4 and V3.0 (BSC 2003a, Section 6.4.5). This addresses a potential mass-balance problem for handling the unreacted solutes in the dryout zone that was present in an earlier version of TOUGHREACT.

The improvements made to TOUGHREACT for handling unreacted solutes are discussed below in detail. In certain cases of evaporation or boiling, a gridblock may experience an influx of water that evaporates completely during the solution of the flow equations. After the flow equations are solved, TOUGHREACT solves the transport equations followed by the speciation and reaction equations. The speciation and reaction equations require that the gridblock is wet; that is, the liquid saturation is greater than zero (or a small value). Because of the lack of water in the gridblock, a method was developed for storing all residual aqueous species in a solid mineral assemblage. This method was developed in order to address the issue of potential mass loss at the boiling front and is summarized below.

The amount of solute stored is simply the product of the concentration in the upstream gridblock and the flux of water into the gridblock that dries out. Also, any water that is initially present in the gridblock and dries out gives rise to some solute mass that is transformed into solid phases. For these cases, the mass of each primary solute species is saved and is assigned to minerals in a prescribed order in the chemical input file. This approximation is performed so that solute mass loss is minimized and nearly all of the solute mass can be accounted for in a solid mineral phase.

TOUGHREACT V2.4 and V3.0 have this option, whereas V2.2 and V2.3 did not. The masses of any remaining solutes not captured by this approach are saved in an output file.

In the simulations presented in *Drift-Scale Coupled Processes (DST and THC Seepage) Models* (BSC 2003a) for the specific cases when water flows into gridblocks that dry out in the flow calculation (by boiling or evaporation), the following solid phases are formed, stoichiometrically and in the following order: silica, calcite, gypsum, hematite, fluorite, NaNO_3 , K_2SO_4 , Na_2SO_4 , MgSO_4 , halite, and sylvite. The order is predetermined (i.e., nitrates are formed before chlorides) to ensure nitrate mass is not lost in cases where insufficient sodium remains to form NaNO_3 (in the absence of other nitrate salts that could have formed). The method was designed to precipitate as much of the dissolved constituents as possible for gridblocks that completely dry out. Upon rewetting, the highly soluble salt minerals (i.e., NaNO_3 , K_2SO_4 , Na_2SO_4 , MgSO_4 , halite, and sylvite) are assumed to dissolve kinetically with a relatively fast rate constant (set to 10^{-6} moles per m^2/s (BSC 2003a)) and a dissolution rate limited by their solubility (BSC 2003a, Section 6.4.2).

F.3.1.2 Mineral Alteration

Precipitation of minerals in the dryout zone and adjacent area affects porosity and permeability. Mineral precipitation leads to porosity and permeability changes in both the fractures and the rock matrix. Minerals commonly seen precipitated in fractures are amorphous silica and calcite (BSC 2003a, Section 6.8.5.4, Figures 6.8-43 to 6.8-46). The precipitation of these minerals results from the repeated boiling and refluxing of condensation water in fractures, in which Ca^{2+} and silica are favorably concentrated because of the dissolution of previously existing fracture minerals, such as calcite and cristobalite.

The most significant minerals precipitating in the matrix are illite (a clay mineral) and stellerite (a zeolite mineral) (BSC 2003a, Section 6.8.5.4). These secondary minerals form from the alteration of the original minerals in the devitrified tuff, such as potassium feldspar and plagioclase. The difference in mineral alteration in fractures and in the rock matrix results from the much lower permeability of the matrix and, hence, a limited exchange of water between fractures and matrix. Additionally, the initial mineralogy in the fractures is different as a result of greater percolation of water since the tuffs were formed.

F.3.1.3 Porosity and Permeability Changes

Thermal-hydrologic simulation, without considering chemical processes, shows the capillary barrier effect of the drift. In fractures, liquid saturations (BSC 2003a, Figure 6.5-5) show the effects of strong diversion of water around the dryout zone. The predicted liquid saturations at 2,400 years, well after the end (at about 1,000 years) of the boiling phase, indicated that ambient water percolation is deflected around the drift. The result is that liquid saturation in fractures is somewhat increased above the drift crown and significantly decreased below the drift (in the shadow zone), in comparison with ambient values away from the drift (BSC 2003a, Figure 6.8-39, Section 6.8.5.4).

The rock-property changes caused by the mineral precipitation leads to flow pattern alterations. Modeling results show that the fracture porosity decreases by approximately 4% to 7%. The

maximum porosity decrease occurs in a thin zone around the drift during reflux at the edge of the dryout zone (BSC 2003a, Section 6.8.5.4). By 2,400 years following waste emplacement, most fractures have rewetted, and the amount of precipitated solids remains essentially unchanged for the remainder of the simulated time period of 100,000 years (BSC 2003a, Figure 6.8-46). The matrix porosity change, with maximum amounts around 1% (BSC 2003a, Section 6.8.5.4), is smaller than the fracture porosity change. THC simulation shows that after the same simulated time period, a zone of higher liquid saturation has formed 7 to 8 m above the drift, reflecting partial diversion of flow at this location. This effect of water diversion results from a thin region of significantly lower permeability (BSC 2003a, Figure 6.8-41a, b) created by prior mineral deposition at the boiling front. As a result, the shadow zone (below the drift) extends somewhat deeper below the drift, and liquid saturations at the drift crown are somewhat reduced, compared to the thermal-hydrologic simulation results. The bases for the discussions regarding the evolution of the unreacted species and the resulting porosity and permeability modification are given in Sections F.4.2 and F.4.3.

F.3.2 Thermal-Hydrologic-Chemical Model Validation

The porosity and permeability changes in the fractured tuffs involve dissolution and precipitation of minerals under elevated heating conditions. Validation of the THC processes in the modeling was done using results from the in situ Drift Scale Test at the Exploratory Studies Facility (BSC 2003a, Section 7.1). In addition, indoor laboratory experiments were performed to observe the dissolution and precipitation in the fractured tuffs (BSC 2003a, Section 7.2) and the effect of precipitated minerals on fracture permeability because of condensation-water refluxing in fractures (BSC 2003a, Section 7.3).

The Drift Scale Test was located at the Exploratory Studies Facility Alcove 5, with nine electrical floor canister heaters placed to simulate nuclear-waste-bearing containers. The Drift Scale Test heaters were activated for a period of about 4 years (from December 1997 to January 2002), which is being followed by 4 years of cooling. The purpose of the test is to evaluate the coupled thermal, hydrologic, chemical, and mechanical processes that take place in unsaturated fractured tuff over a range of temperatures (approximately 25°C to 200°C). The THC model (BSC 2003a, Section 7.1) has been validated against the Drift Scale Test data of the heating phase for thermal and hydrologic evolution, gas-phase CO₂ evolution, aqueous species evolution, mineralogical changes, and porosity and permeability changes (BSC 2003a, Sections 7.1.9-13). Calcite, amorphous silica, and a calcium sulfate phase are the only solid phases identified from the samples as products of the processes that took place during the heating phase of the Drift Scale Test. The fracture volume filled by minerals is estimated to be less than 1%.

Two other validation studies include a laboratory plug-flow reactor experiment (BSC 2003a, Section 7.2) and a fracture sealing experiment (BSC 2003a, Section 7.3). These two experiments were conducted at elevated temperatures to emulate the waste emplacement heat loading and to produce the effects of the boiling, evaporation, and condensation processes. The purposes of these two experiments are to investigate the effect of THC processes on the dissolution and precipitation of rock minerals of Yucca Mountain tuffs and to investigate fracture sealing caused by the precipitation of minerals on the fracture walls. A detailed description of these validation tests is given in Section F.4.4.

F.3.3 Thermal Alteration in the Calico Hill Nonwelded Hydrologic Unit

Thermal effects on locations beyond the surrounding area of the drift, such as the Calico Hill nonwelded hydrologic (CHn) unit, have been included in the THC simulations in Revision 2 of *Drift-Scale Coupled Processes (DST and THC Seepage) Models* (BSC 2003a, Table 6.7-1), by extending the model domain beyond the CHn unit to the water table. These simulations have considered chemical reactions that cause mineralogical alterations (e.g., precipitation or dissolution), porosity modification, and resulting permeability change. Relevant THC processes accompanying the temperature rise in the CHn unit are thus captured. Results from mountain-scale THC models indicate that alteration of the CHn vitric and zeolitic units are caused by the thermal effects of waste emplacement; however, the resulting hydrologic property changes are insignificant (BSC 2003b, Sections 6.4.3.3.3, 6.4.3.3.4). Under long-term heating, the potential changes of the CHn vitric tuffs and clay mineral phases and of the hydrologic properties are considered small because the temperature rise at the CHn unit is small and localized below the repository drifts. Simulations of chemical alteration in the CHn unit show a 1% increase in porosity, which would not be expected to significantly change permeability in the unit. Therefore, the impact from chemical alteration of the CHn unit on repository performance is expected to be small.

The basis for considering thermal effects on the CHn unit is given in Sections F.4.1.1, F.4.2, and F.4.5.

The information in this report is responsive to AIN request ENFE 1.03 AIN-1. This report contains the information that DOE considers necessary for NRC review for closure of this agreement.

F.4 BASIS FOR THE RESPONSE

The repository hydrogeologic model units include the Topopah Spring welded (TSw) upper lithophysal (Ttpul), middle nonlithophysal (Ttpmn), and lower lithophysal (Ttpll) units (model units tsw33, tsw34, and tsw35, respectively). Most hydrogeologic data available for the repository horizon are from the highly fractured Ttpmn unit, including data from the Single Heater Test, the Drift Scale Test, and many other data collected in the Exploratory Studies Facility (BSC 2003a, Section 6.5). However, only part of the repository is planned to be located in the Ttpmn unit. Most of the repository is planned to be located in the Ttpll unit (BSC 2003a, Sections 6.3 and 6.5). The Ttpll lithostratigraphic unit differs significantly from the Ttpmn unit in that it includes a significant number of lithophysal cavities, which are accounted for with revised thermal properties for lithophysal porosity (BSC 2003a, Section 6.8). Simulations using the Ttpmn unit as host layer are used as sensitivity studies. Simulations treating the Ttpll unit as the repository host layer are delivered for downstream users for the TSPA.

The data necessary for the evaluation of THC processes include (1) unsaturated hydrologic properties, (2) initial and boundary water and gas chemistry, (3) initial mineralogy, mineral volume fractions, and reactive surface areas, (4) equilibrium thermodynamic data for minerals and aqueous and gaseous species, (5) kinetic data for mineral-water reactions, and (6) diffusion coefficients for aqueous and gaseous species (BSC 2003a, Section 6.2.1). Data derived from

field and laboratory experiments include unsaturated hydrologic properties, mineral composition, water, and gas chemistry data. Other data are collected from literature or theoretical calculation (BSC 2003a, Sections 4.1, 6.4, and 6.8.3).

Revision 0 of *Drift-Scale Coupled Processes (DST and THC Seepage) Models* (CRWMS M&O 2000) presented THC simulations of the Drift Scale Test and a THC seepage model (Tptpmn THC backfill model), which were retained and not changed in Revision 1 of that report (BSC 2002a, Section 6.2). Revision 1 (BSC 2002a) includes three additional models (Tptpmn THC no-backfill model, Tptpmn THC heterogeneous model, and the Tptpll THC model) and model validation using plug-flow reactor data.

Major changes in Revision 2 of *Drift-Scale Coupled Processes (DST and THC Seepage) Models* (BSC 2003a) include new simulations that make use of improved treatment of various modeled processes, together with updated hydrologic and thermal properties and some new kinetic and thermodynamic input data. In addition, Revision 2 further evaluates the uncertainties associated with the results of the THC seepage model through considering five input water compositions, variations in infiltration rates, increase of CO₂ effective diffusivity (BSC 2003a, Section 6.8.3), and the effect of vapor-pressure lowering (caused by capillary pressure) (BSC 2003a, Section 1.1). The model validation of Revision 2 includes the Drift Scale Test and a fracture sealing experiment, in addition to the plug-flow reactor experiment in Revision 1 of the report (BSC 2002a).

The repository drift-scale THC seepage model is used in support of the TSPA in-drift geochemical model. Results from the Tptpll THC model Revision 2 results (BSC 2003a, Section 1.1) are abstracted for inclusion in *Abstraction of Drift-Scale Coupled Processes* (BSC 2003c) for the TSPA. The Tptpll THC model (Revision 2) was run using a range of input water compositions that were measured in various lithostratigraphic units (including Tptpmn, Tptpll, and Tptpul) to represent natural variability. The spread in model results from the use of these different water compositions is mostly a result of the spread related to other factors, such as drift location and infiltration rate, and other model conceptualizations discussed in *Drift-Scale Coupled Processes (DST and THC Seepage) Models* (BSC 2003a, Section 6.3). The Revision 2 model results for the Tptpll unit (taking into account the variability introduced by the different input water compositions) are applicable to other repository host-rock units (BSC 2003a, Section 1.2). The new features in Revision 2 of the Tptpll THC model (BSC 2003a, Section 6.8), compared to Revision 1 of the Tptpll model, are a drift wall open to gas and liquid flow, fixed infiltration rate, and the effect of vapor-pressure lowering (resulting from capillary pressure).

The rationale for the KTI response is divided into five parts. Section F.4.1 describes the dual-permeability method and model mesh, the thermal-hydrologic and THC processes, and infiltration water, gas, and mineral data. Section F.4.2 discusses the thermal-hydrologic and THC simulations and results. Section F.4.3 presents the analyses of simulated mineral alteration and porosity and permeability changes. Section F.4.4 contains the THC model validation. Section F.4.5 provides the basis for the response to the comment regarding thermal alteration of the CHn unit.

F.4.1 Thermal-Hydrologic-Chemical Process Model

This section describes the THC modeling, including the dual continuum modeling approach, the THC processes, and pore water, gas, and mineral data for the simulations.

F.4.1.1 Dual-Permeability Method

The dual permeability method (Wu et al. 2002) is used for describing flow and transport in the drift-scale THC model (BSC 2003a, Section 6.2.1.5). In the dual-permeability model, each gridblock is partitioned into matrix and fracture continua, each characterized by its own pressure, temperature, liquid saturation, water and gas chemistry, and mineralogy. Simulations were performed on a vertical two-dimensional mesh representing a half-drift model with a width of 40.5 m (corresponding to distance between the drift center and the midpoint between drifts) and a drift diameter of 5.5 m. The bottom boundary in Revision 2 of the model (BSC 2003a) extends beyond the CHn unit to the water table. The mesh has 3,202 gridblocks, including those representing matrix, fracture, and in-drift design elements (BSC 2003a, Section 6.7.1, Figure 6.7-1).

F.4.1.2 Thermal-Hydrologic-Chemical Processes

In the conceptual thermal-hydrologic model, heating results in vapor migration away from the area surrounding the heat source. Heat is conducted from the drift wall into the rock matrix. In the vicinity of the drift, the vapor moves away from the drift through the permeable fracture network after vapor migrates out of the matrix and into the fractures. Consequently, continual heating will result in development of a dryout zone in the vicinity of the drift. When vapor enters the cooler regions, it condenses on fracture walls and drains through fracture networks (BSC 2003a, Section 6.2.1.1).

The effects of thermal-hydrologic processes on water chemistry are varied and depend on the physical and chemical properties of the dissolved species and relevant mineral–water reactions. Conservative species, such as chloride (Cl^-), become concentrated in waters that are undergoing vaporization or boiling. Concentrations of aqueous species, such as calcium (Ca^{2+}), are affected by calcite dissolution or precipitation, as well as by reactions involving calcium-bearing zeolites, clays, and plagioclase feldspar. Water vapor is transported from the boiling zone to the zone where it condenses (the condensation zone). CO_2 is depleted in pore water at the boiling zone because of outgassing (exsolution), leading to a local increase of pH; CO_2 is enriched in the condensate in the condensation zone, resulting in a local decrease of pH. Condensed water in the fracture system is the active front where mineral dissolution and precipitation, as well as direct interaction between matrix pore waters and fracture waters, occur (BSC 2003a, Section 6.2.1.2).

F.4.1.3 Compositions of Infiltration Water, Gases, and Minerals

In the initial version of *Drift-Scale Coupled Processes (DST and THC Seepage) Models* (CRWMS M&O 2000), the availability of infiltrating water data was limited to three pore-water samples, collected from the highly fractured middle nonlithophysal zone (Ttptmn) geologic unit in Alcove 5 near the Drift Scale Test (BSC 2003a, Section 6.2.2.1). Since then, a series of pore-water samples from repository host units have been collected and analyzed in the Enhanced Characterization of Repository Block (ECRB) Cross-Drift and in boreholes USW SD-9, USW

NRG-7, and USW NRG-7a (BSC 2003a, Section 6.2.2.1). In Revision 2 of *Drift-Scale Coupled Processes (DST and THC Seepage) Models* (BSC 2003a), five types of infiltrating waters were chosen, with preference given to actual pore waters from unsaturated regions within or above the repository units (BSC 2003a, Section 6.2.2.1).

The following water compositions were selected, listed here with an arbitrary identification (W0, W5, etc.) assigned for the THC seepage model (BSC 2003a, Section 6.2.2.1, Figure 6.2-4):

- **W0**—Water sample from the Tptpmn unit in Alcove 5
- **W4**—Sample from the Tptpll lithostratigraphic unit in the ECRB Cross-Drift
- **W5**—Sample from the base of the Tptpul lithostratigraphic unit in the ECRB Cross-Drift
- **W6**—Sample from the Tptpll lithostratigraphic unit in borehole USW SD-9
- **W7**—Sample from the Tptpul lithostratigraphic unit in the ECRB Cross-Drift.

The choice of input water composition also involves considerations of the natural variability of pore-water compositions in the repository units. Different initial water concentrations may result in the development of different brines with evaporation (BSC 2004).

Waters such as those from USW UZ-14 pore water and J-13 well water are excluded because they appear to be dramatically different from pore waters in the repository units, even though they appear to be end-members of waters from Yucca Mountain and vicinity. However, this type of water with low pore-water concentrations and very low $(Ca+Mg)/(Na+K)$ ratios may have existed in the repository horizon, as revealed in a recent analysis of pore water (Lu et al. 2003, Section 4.4; Gascoyne 2003). Because of the low $(Ca+Mg)/(Na+K)$ ratios, the pore waters with low water concentrations (i.e., J-13 under evaporation) would lead to development of less deleterious brines such as sodium chloride, or brines that are less hygroscopic (having the ability to absorb water from the air), rather than potentially more deleterious brines such as calcium and magnesium chloride (BSC 2003d).

Overall, the five infiltrating waters were selected from available water samples at Yucca Mountain and are, therefore, representative of unsaturated pore water. Simulation results using these types of waters are on the conservative side because the waters tend to form more deleterious brines under evaporation. Details on the aqueous species, gases, and major solid phases within the geologic units can be found in *Drift-Scale Coupled Processes (DST and THC Seepage) Models* (BSC 2003a, Section 6.2.2.2).

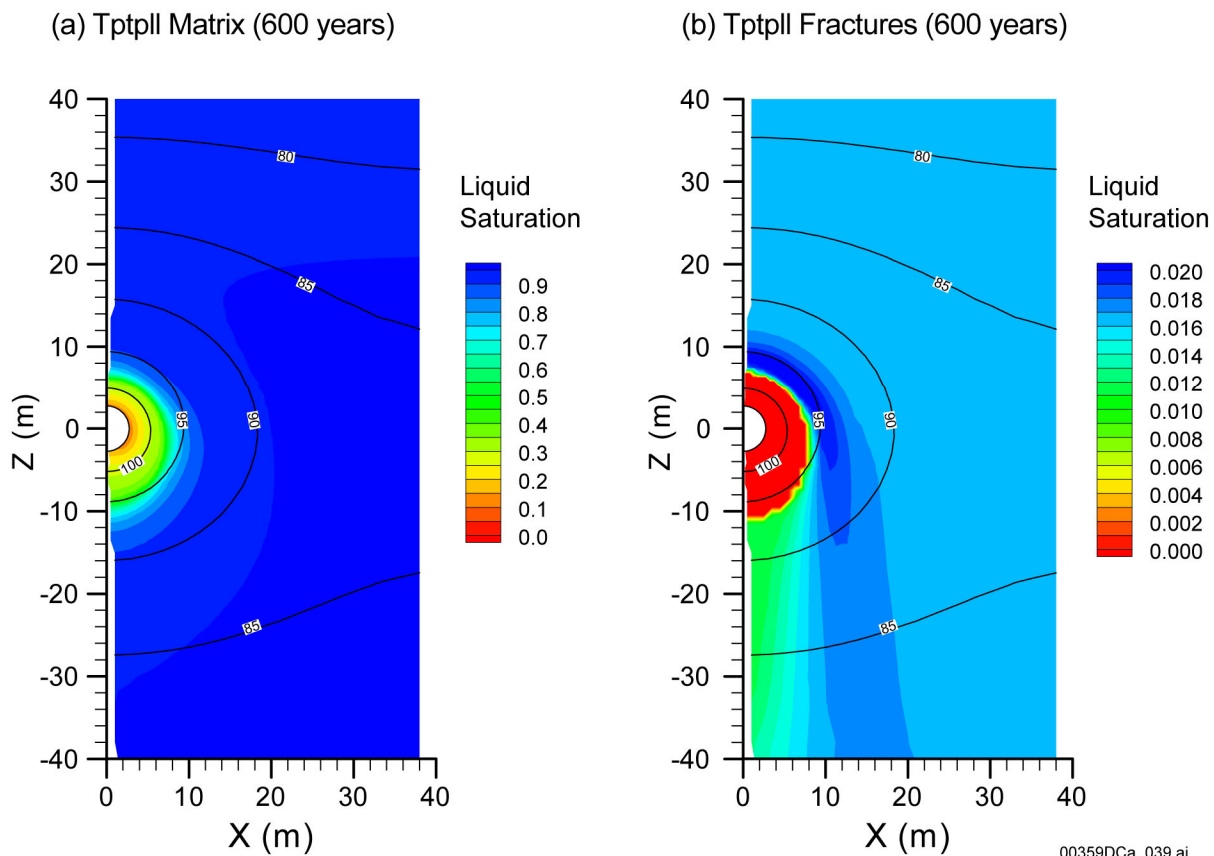
F.4.2 Pore-Water Thermal-Hydrologic-Chemical Evolution

This section discusses the temperature distribution and saturation around the drift and capillary barrier. The dryout zone formed under thermal loading is delineated and the evolution of water chemistry is then reviewed. The simulation period lasts for 100,000 years, with drift ventilation for the first 50 years, and ventilation cessation at closure. In the simulations, the infiltration rates vary over time, using 6, 16, and 25 mm/yr, from 0 to 600 years (present day), 600 to 2,000 years

(monsoon), 2,000 to 100,000 years (spanning the glacial-transition (2,000 to 20,000 years) and glacial period (more than 20,000 years)), respectively (BSC 2003a, Table 6.5-3; BSC 2003e, Section 6.9).

F.4.2.1 Saturation and Dryout Zone

The thermal-hydrologic model results show that the temperature quickly increases after the cessation of ventilation at 50 years. Then the temperature at the drift walls is maintained above 96°C (approximate boiling point at the modeled elevation) until about 2,000 years. The thermal pulse of waste thermal loading is significantly lowered after 10,000 years and completely dissipates at 100,000 years (BSC 2003a, Figure 6.5-3, Section 6.5.5.1). Figure F-1 shows the spatial distribution of temperature and saturation around the drift at 600 years for the thermal-hydrologic simulation.



Source: BSC 2003a, Figure 6.8-6.

NOTE: Rewetting of the matrix at the drift wall has already occurred (BSC 2003a, Figure 6.8-8).

Figure F-1. Plot of Modeled Temperatures and Liquid Saturations of the Thermal-Hydrologic Model (Revision 2) at 600 Years (near the Time of Maximum Dryout in Fractures) in the Dual Continua: (a) Matrix, and (b) Fractures

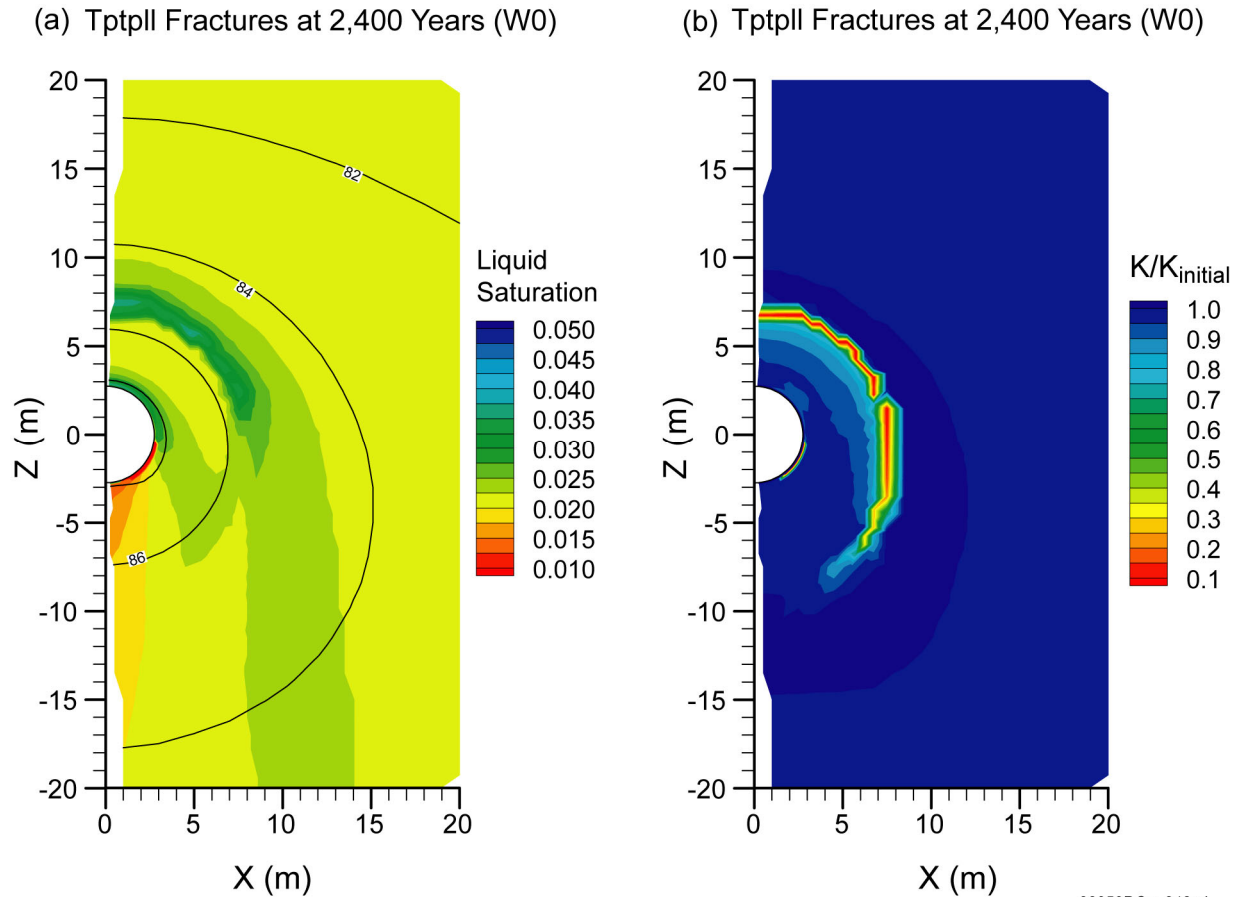
The thermal-hydrologic processes form a dryout zone (as defined by zero saturation) around the drift. The maximum extent of the dryout zone for fractures is approximately 12 m below the

drift, 9 m to the side, and 8 m above drift center; the dryout zone for the matrix is smaller (Figure F-1) (BSC 2003a, Section 6.7.5.1, Figure 6.7-4).

In fractures, liquid saturations (BSC 2003a, Figure 6.5-5) show evidence of strong water diversion around the dryout zone. The maximum dryout in fractures occurs near 600 years. This is also the time at which the model infiltration rate increases from 6 to 16 mm/yr (BSC 2003a, Section 6.7.5.1).

In addition to the smaller extent of dryout in the rock matrix, the matrix rewets much earlier than fractures. Matrix and fractures behave differently because of the effect of vapor-pressure lowering on matrix saturation. The effect of vapor-pressure lowering caused by capillary pressure makes it possible for a liquid phase to exist under conditions where vapor partial pressure and gas phase total pressure are less than the saturation pressure (Pruess et al. 1999, p. 38). The model with vapor-pressure lowering shows that the extent of dryout in the matrix is smaller than that in fractures, even though temperatures are essentially the same in both media (Figure F-1; also compare *Drift-Scale Coupled Processes (DST and THC Seepage) Models* (BSC 2003a, Figure 6.7-4) without vapor-pressure lowering). Pressure lowering affects the rewetting of the locations around the drift wall (about 10 to 20 cm into the rock) (for locations, see BSC 2003a, Section 6.5.5, Figure 6.5-2). The rock matrix at the drift wall rewets at around 200 to 300 years, much earlier than that in previous models without vapor-pressure lowering (at 1,200 to 1,400 years) (BSC 2003a, Section 6.8.5.2, Figure 6.8-8). Note that temperatures at the drift wall peak at around 120°C to 140°C (the highest temperature of the waste package is near 155°C) between 55 and 75 years (BSC 2003a, Section 6.5.5.1, Figures 6.5-3, 6.8-4). The fractures rewet at around 1,000 to 1,500 years (BSC 2003a, Section 6.8.5.2, Figure 6.8-7). However, the time of rewetting around the drift wall is similar for models both with and without vapor-pressure lowering (BSC 2003a, Sections 6.8.5.2, Figure 6.8-7).

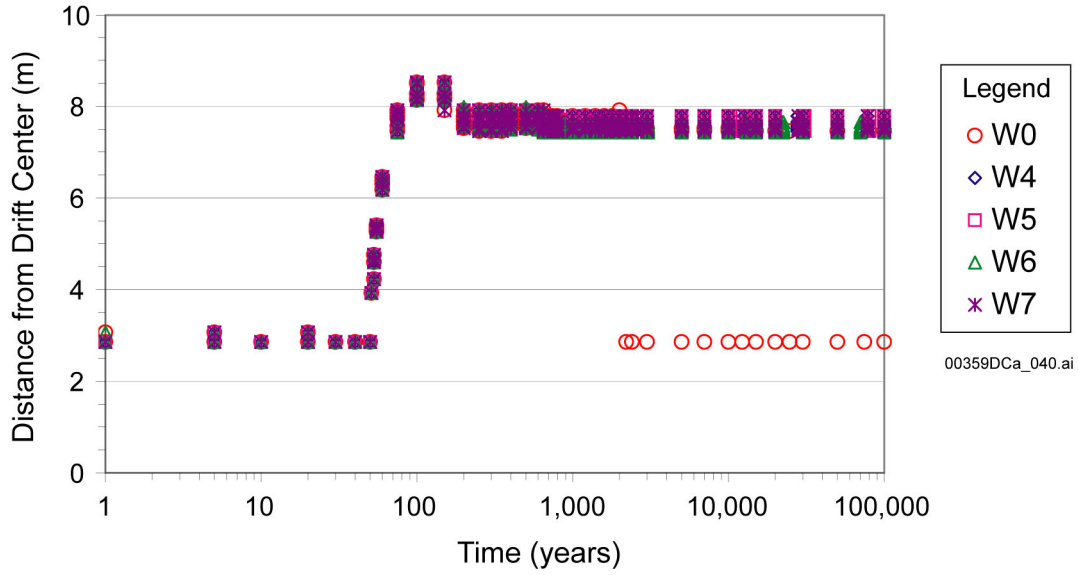
The high-saturation zone is used to demonstrate the chemical evolution of pore waters. This zone generally moves away from the drift as moisture is driven away by the heat source. From the onset of boiling at approximately 50 years, the high saturation zone is associated with condensation (reflux) above the drift. At the later time shown in Figure F-2, the high-saturation zone is adjacent to zones of reduced permeability formed by prior mineral deposition at the boiling front. Some high-saturation data points are directly adjacent to the drift crown (some W0 data points on Figure F-3). Description of these zones is provided in *Drift-Scale Coupled Processes (DST and THC Seepage) Models* (BSC 2003a, Section 6.8.5.4).



Source: BSC 2003a, Figure 6.8-40.

Figure F-2. Thermal-Hydrologic-Chemical Simulation (Tptpll Water W0): Contour Plot of Modeled (a) Liquid Saturation and Temperature Contours and (b) Permeability Change in Fractures at 2,400 Years

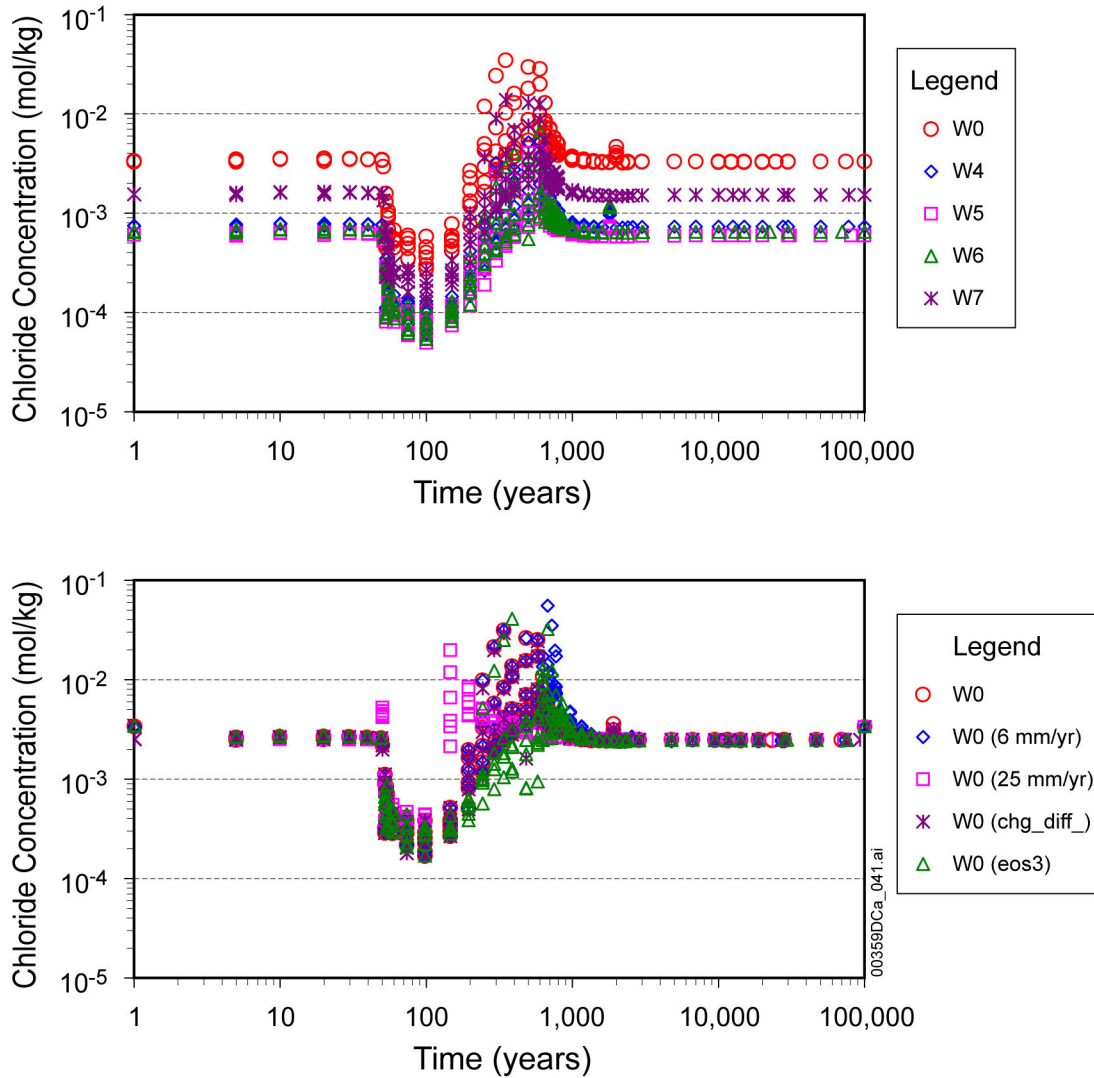
In the discussion of the THC simulations, which includes Figures F-4 through F-8, the data points of pore water chemistry were taken from the model gridblocks that have the highest liquid saturation in fractures located above the drift crown within a 45-degree arc (BSC 2003a, Section 6.8.5.3.2). The locations of these points for the five types of pore water compositions are shown in Figure F-3.



Source: BSC 2003a, Figure 6.8-22 (top figure).

NOTE: The locations were determined from the gridblocks that have the highest saturation at a specific time. They are obtained from area within 25-m range from the drift center and a 45-degree arc from the drift crown. Data are shown for simulations using different initial water compositions (W0 to W7). These gridblocks are the actual locations of the data points shown in Figures F-4 to F-8.

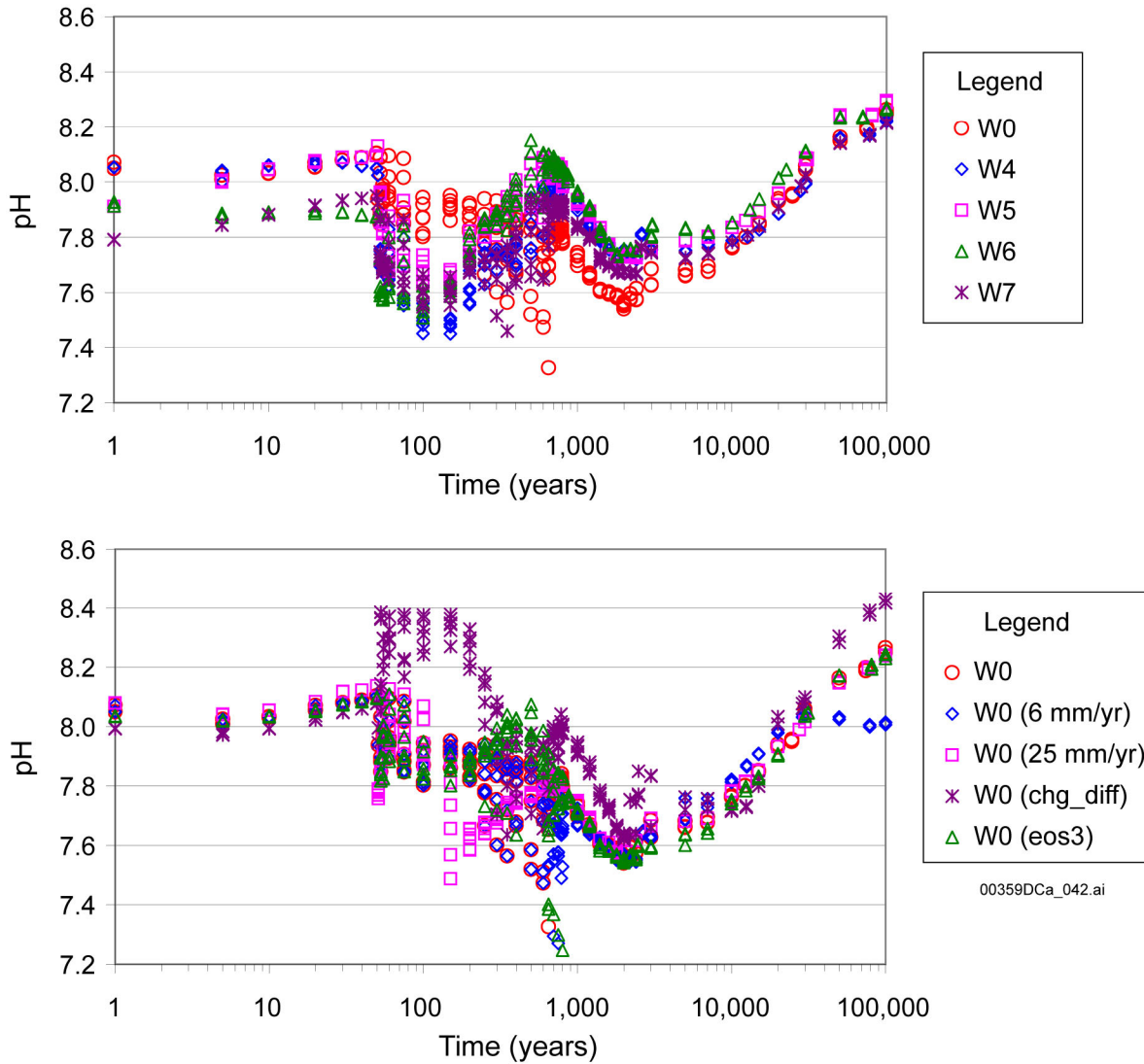
Figure F-3. Locations of the Model Gridblocks for the Highest Liquid Saturation in Fractures near the Drift Crown



Source: BSC 2003a, Figure 6.8-28.

NOTE: These data were obtained from the gridblocks that have the highest saturation at a specific time (Figure F-3). All simulations were run using a stepwise-increasing infiltration rate (6, 16, and 25 mm/yr for 0 to 600, 600 to 2,000, and 2,000 to 100,000 years, respectively) and with vapor-pressure lowering, with the exceptions as followed. Data for W0 6 mm/yr and W0 25 mm/yr come from simulations with fixed 6 and 25 mm/y infiltration rates, W0 chg_diff with CO₂ diffusion coefficient increased six-fold, and (W0 eos3) without vapor-pressure lowering.

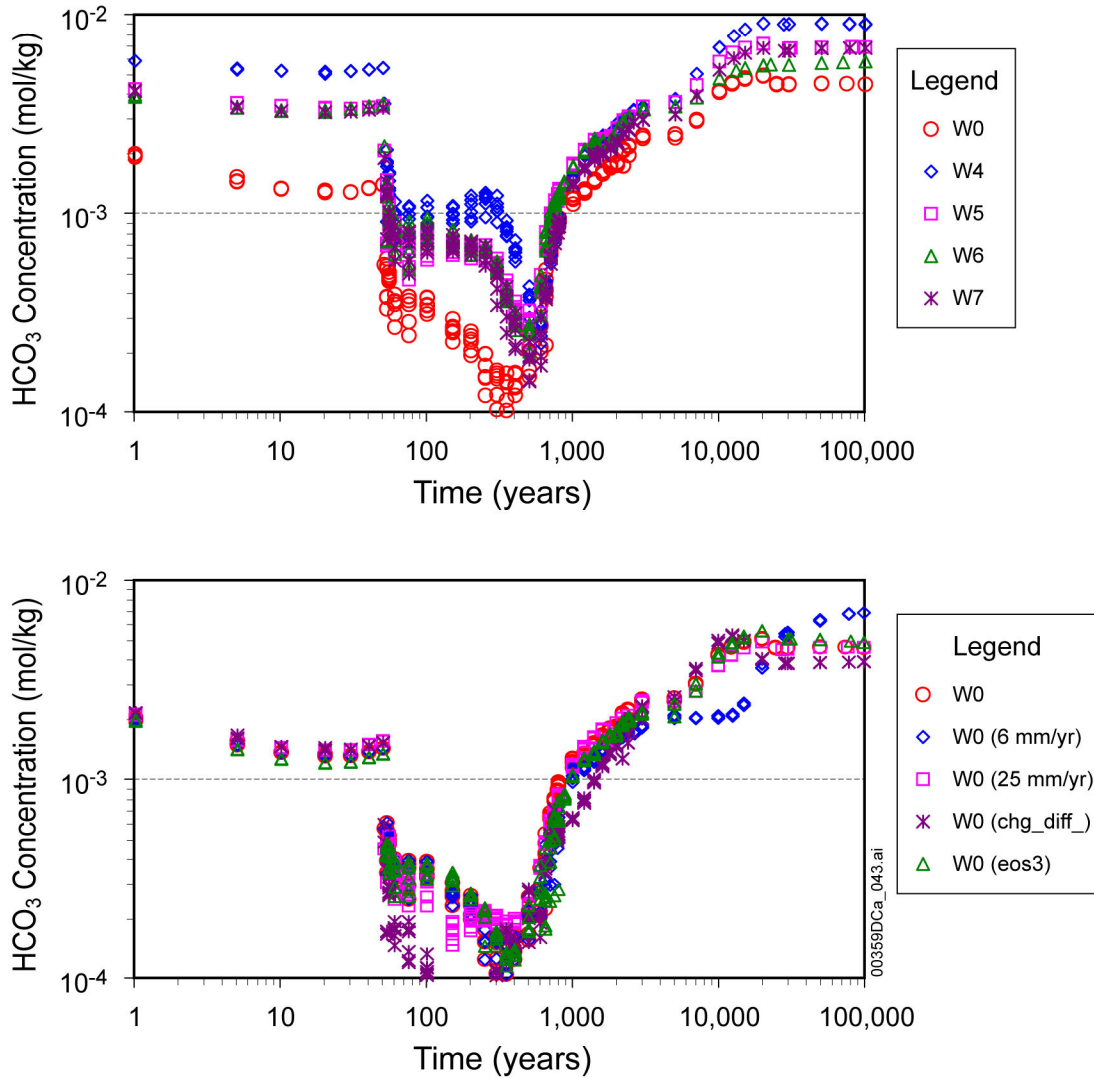
Figure F-4. Time Profiles of Modeled Total Aqueous Chloride Concentrations in Fracture Water in Areas of Highest Liquid Saturation above the Drift Crown



Source: BSC 2003a, Figure 6.8-26.

NOTE: These data were obtained from the gridblocks that have the highest saturation at a specific time (Figure F-3). Simulations were run using a stepwise-increasing infiltration rate (6, 16, and 25 mm/yr for 0 to 600, 600 to 2,000, and 2,000 to 100,000 years, respectively) and with vapor-pressure lowering, with the exceptions as followed. Data for W0 6 mm/yr and W0 25 mm/yr come from simulations with fixed 6 and 25 mm/yr infiltration rates, W0 chg_diff with CO₂ diffusion coefficient increased by six-fold, and (W0 eos3) without vapor-pressure lowering.

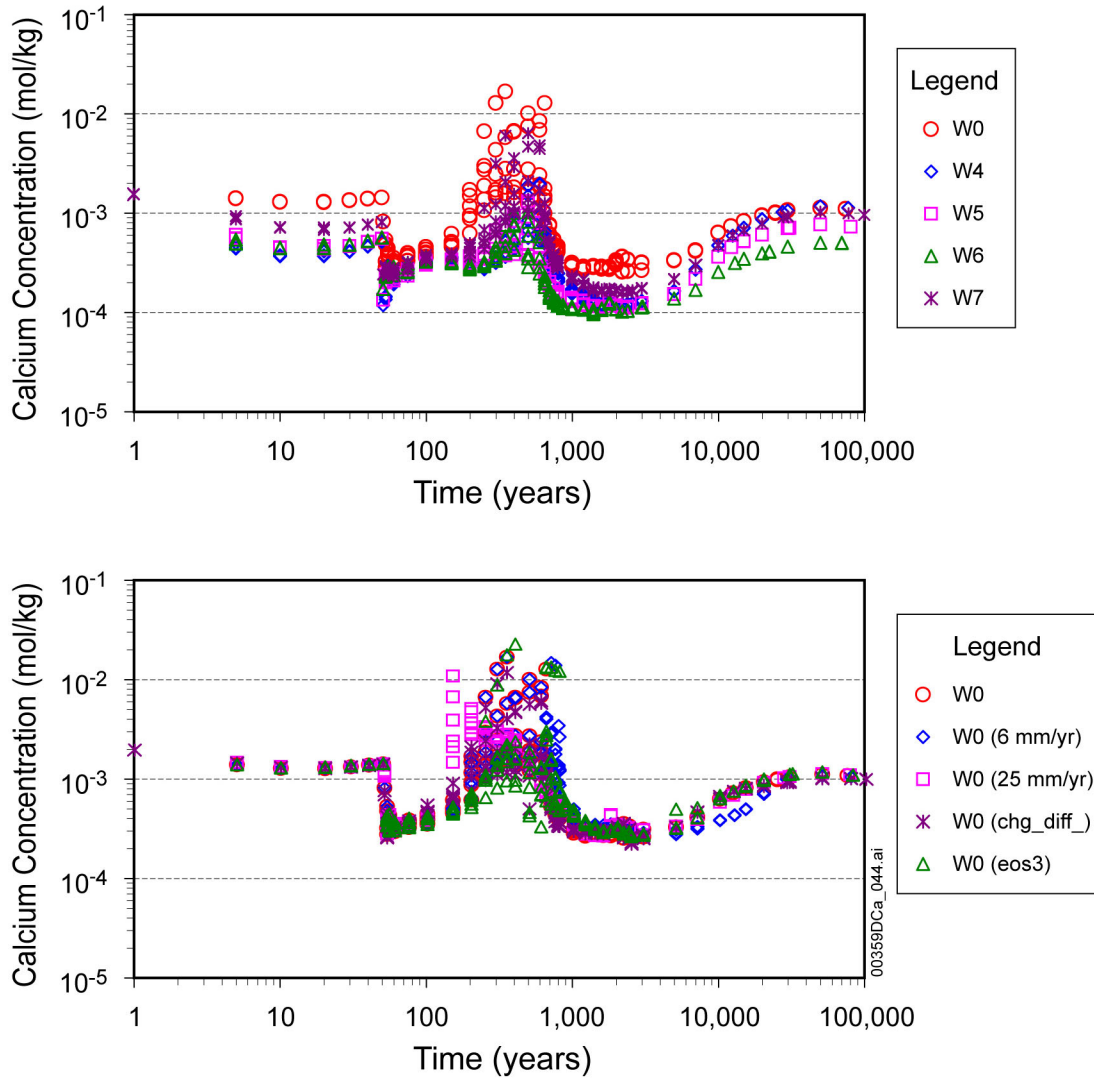
Figure F-5. Time Profiles of Modeled pH in Fracture Water in Areas of Highest Liquid Saturation above the Drift Crown



Source: BSC 2003a, Figure 6.8-27.

NOTE: These data were obtained from the gridblocks that have the highest saturation at a specific time (Figure F-3). Simulations were run using a stepwise-increasing infiltration rate (6, 16, and 25 mm/yr for 0 to 600, 600 to 2,000, and 2,000 to 100,000 years, respectively) and with vapor-pressure lowering, with the exceptions as followed. Data for W0 6 mm/yr and W0 25 mm/yr come from simulations with fixed 6 and 25 mm/yr infiltration rates, W0 chg_diff with CO₂ diffusion coefficient increased by six-fold, and (W0 eos3) without vapor-pressure lowering.

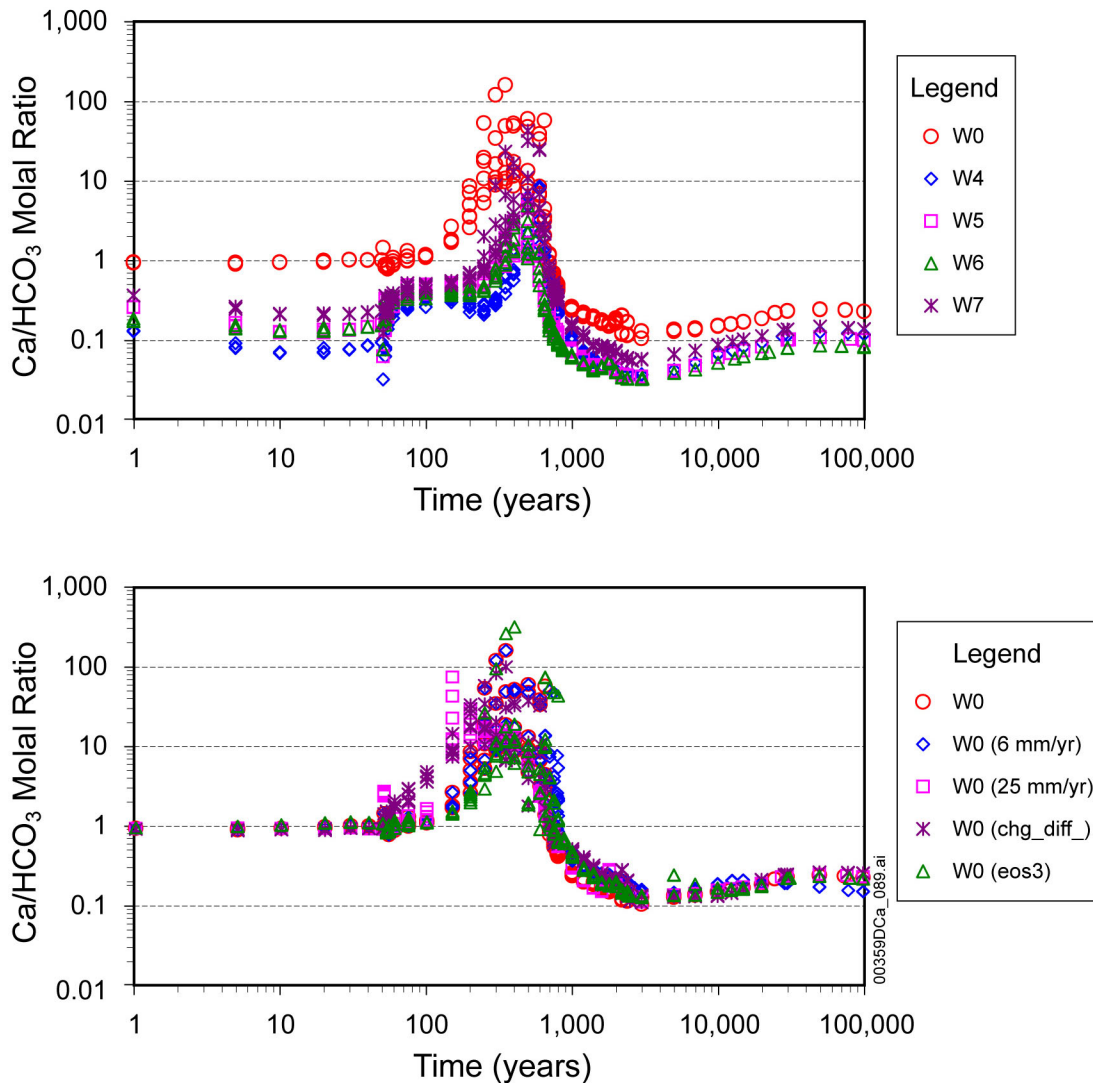
Figure F-6. Time Profiles of Modeled Total Aqueous Carbonate Concentrations (as HCO₃) in Fracture Water, in Areas of Highest Liquid Saturation above the Drift Crown



Source: BSC 2003a, Figure 6.8-30.

NOTE: These data were obtained from the gridblocks that have the highest saturation at a specific time (Figure F-3). Simulations were run using a stepwise-increasing infiltration rate (6, 16, and 25 mm/yr for 0 to 600, 600 to 2,000, and 2,000 to 100,000 years, respectively) and with vapor-pressure lowering, with the exceptions as followed. Data for W0 6 mm/yr and W0 25 mm/yr come from simulations with fixed 6 and 25 mm/y infiltration rates, W0 chg_diff with CO₂ diffusion coefficient increased by six-fold, and (W0 eos3) without vapor-pressure lowering.

Figure F-7. Time Profiles of Modeled Total Aqueous Calcium Concentrations in Fracture Water, in Areas of Highest Liquid Saturation above the Drift Crown



Source: BSC 2003a, Figure 6.8-34.

NOTE: These data were obtained from the gridblocks that have the highest saturation at a specific time (Figure F-3). Simulations were run using a stepwise-increasing infiltration rate (6, 16, and 25 mm/yr for 0 to 600, 600 to 2,000, and 2,000 to 100,000 years, respectively) and vapor-pressure lowering, with the exceptions as follows: data for W0 6 mm/yr and W0 25 mm/yr come from simulations with fixed 6 and 25 mm/y infiltration rates, W0 chg_diff with CO₂ diffusion coefficient increased by six-fold, and (W0 eos3) without vapor-pressure lowering.

Figure F-8. Thermal-Hydrologic-Chemical Simulations (Tptpl Model Revision 2): Time Profiles of Modeled Total Aqueous Calcium to Carbonate Ratios in Fracture Water, in Areas of Highest Liquid Saturation above the Drift Crown

F.4.2.2 Chemical Evolution of Pore Waters

The concentration profiles of conservative species, such as chloride (Figure F-4) and nitrate (BSC 2003a, Figures 6.8-28 and 6.8-29), are useful in evaluating the degree of dilution and evaporative concentration in the high liquid saturation areas. Nitrate is included in the present simulations, in contrast to Revision 1 (BSC 2002a) simulations, where it was omitted. Nitrate is

treated as a conservative species (BSC 2003a, Section 6.8.5.3.2). Evaporitic precipitates of nitrate and chloride salts are formed only upon complete dryout (BSC 2003a, Section 6.4.5). Other constituents in the pore waters appear as residuals in the dryout phase.

Dilution from condensation by a factor of around 10 initially occurs after the onset of boiling. However, later in the boiling period, concentration increase resulting from evaporation takes over (also by a factor of around 10, compared to initial values). By comparing the chloride concentration profiles (Figure F-4) with profiles showing the distance above the drift center at which these concentrations occur (Figure F-3), the following successive stages in the evolution of water composition in the condensation zone are identified:

1. A dilution stage occurs when the dryout zone is expanding, roughly from 50 to around 100 to 150 years. It is caused by steam originating from water boiling in the rock matrix that migrates to, and condenses in the fractures (BSC 2003a, Section 6.2.1.1). The condensation water refluxes in the fractures at the edge of the fracture dryout zone as ongoing boiling and condensation processes reach equilibrium state.
2. An evaporative concentration stage takes place while the high liquid-saturation zone remains essentially stationary. The aqueous species in the fractures are concentrated as the percolating water boils, with little or no additional influx of condensation water derived from boiling matrix water. This stage lasts from approximately 150 to 600 years for most waters, but is shorter (lasting from 150 to 250 years) for the higher infiltration rate (fixed at 25 mm/yr) (Figure F-4).
3. A back-to-ambient stage starts while boiling is still occurring, after approximately 600 years (and earlier at higher infiltration rates (25 mm/yr)), and then continues after the dissipation of the boiling front. During this stage, the dilution by percolating waters overcomes the effect of evaporative concentration, and concentrations return to their ambient values.

The effects of these three distinct stages are visible on the simulated concentration trends of most constituents. In the case of chloride, concentrations drop to as low as around 1 ppm (with water W6) during the dilution stage and rise to as high as nearly 1,500 ppm (with water W0) during the evaporative concentration stage (Figure F-4).

The simulated pH values (Figure F-5) are within a narrow range, from approximately 7.2 to 8.4. After long periods of time (greater than 10,000 years), pH values for runs using the different input water compositions tend to converge toward similar ambient values (in the 8.2 to 8.4 range at 100,000 years) (Figure F-5). The pH rise toward these ambient values is preceded by a pH decrease (from approximately 600 to 2,000 years), accompanied by increased HCO_3^- concentration (Figure F-6) and drastically decreased Ca^{2+} concentration (Figure F-7) (compare Figure F-8 for Ca/HCO_3 ratio change). The pH decrease is caused by the percolation of more carbonated water (slightly more acidic waters) (Figure F-6).

In zones of highest liquid saturation above the drift crown, increases in Ca/Cl ratios within fractures during the dilution stage (BSC 2003a, Figure 6.8-31) result from calcite dissolution in fractures. This dissolution is enhanced by the somewhat lower pH of condensation waters

caused by increased aqueous CO_2 (BSC 2003a, Section 6.8.5.3.2). The change in pH is caused by the thermal effect on aqueous CO_2 concentrations. The exsolution of CO_2 in the boiling zone results in a local increase in pH and a decrease in pH in the condensation zone into which the vapor enriched in CO_2 is transported and condensed (BSC 2003a, Section 6.2.1.2).

When evaporative concentration takes over, Ca/Cl ratios decrease mainly through precipitation of calcite. The ratio of calcium to total aqueous carbonate concentration (expressed here as Ca/ HCO_3 as shown in Figure F-8) gives some indication of the likelihood for a water to evolve toward a potentially deleterious calcium chloride brine upon continued evaporation. These brines are more likely to form in initial waters with a Ca/ HCO_3 molal ratio greater than 0.5 (or, in equivalents, a ratio greater than 1). These values are exceeded during the evaporative concentration stage for the considered initial water compositions. However, waters W0 and W7 display Ca/ HCO_3 ratios significantly higher than the other waters. Water W4 shows the lowest ratios.

Ratios of nitrate to chloride (BSC 2003a, Figure 6.8-35) remain essentially constant. Solid nitrate phases are formed only upon complete dryout (BSC 2003a, Section 6.4.5). Redox processes are not considered in these simulations because thermodynamics does not favor reduction of nitrate to nitrite in the saturated zone, over which temperature effect plays only a secondary role.

Any water that is initially present in a dryout gridblock gives rise to some solute mass that is transformed into solid phases. To account for the mineral precipitates in the dryout zone, special numerical implementation in TOUGHREACT was developed for storing the residual aqueous species in a solid mineral assemblage. The amount of solute stored is the product of the concentration in the upstream gridblock and the amount of water that flows into the gridblock and dries out. The THC simulations with TOUGHREACT V2.4 and V3.0 have taken into account the unreacted solutes in the dryout zone, thereby fixing the mass balance problem of handling unreacted solutes in the dryout zone in the earlier versions of TOUGHREACT. Relevant detailed discussion can be found in *Drift-Scale Coupled Processes (DST and THC Seepage) Models* (BSC 2003a, Section 6.4.5). Comparison of modeled mineral precipitation in the Drift Scale Test using the earlier version of TOUGHREACT (BSC 2003a, Figure 7.1-35) and TOUGHREACT V3.0 (BSC 2003a, Figure 7.1-37) show that there was a maximum of about a factor of 3 increase in the calcite abundance (although some of this increase was due to a smaller fracture porosity in the latter simulation). More details regarding this comparison can be found in *Drift-Scale Coupled Processes (DST and THC Seepage) Models* (BSC 2003a, Section 7.1.12). THC seepage model simulations using the revised version of TOUGHREACT and its effect on mineral precipitation and permeability changes are discussed in *Drift-Scale Coupled Processes (DST and THC Seepage) Models* (BSC 2003a, Section 6.8.5.4).

Simulations show that dissolved silica concentration (BSC 2003a, Figure 6.8-37) has the same effects of dilution and evaporative concentration as most other species. Profiles of SiO_2 /Cl ratios have the same general shape as the Ca/Cl profiles (BSC 2003a, Figure 6.8-31) and indicate significant silica dissolution during the dilution stage. Later, continued reflux and boiling lead to an increase in concentrations. Concentrations eventually reach values greater than the solubility of amorphous silica (around 350 ppm at 95°C). This is because the calculated precipitation rate

of amorphous silica, although quite fast, is slower than the rate of concentration increase by boiling.

Fluoride concentrations (BSC 2003a, Figure 6.8-38) follow a trend similar to the trend of silica and other aqueous species. The host rock is modeled with a small, widely distributed amount of primary fluorite. Because the dissolution rate of fluorite is fast, waters generally reach saturation with respect to this mineral. During the boiling and refluxing stage, concentrations go up to around 40 ppm, which are much larger than the concentration (about 1.4 ppm) calculated by equilibrating fluorite with the solution, using the maximum calcium concentrations (around 0.02 mol/kg, see Figure F-7) predicted during that time period. Also, in this case, the precipitation rate of fluorite is slower than the rate of concentration increase by boiling. Eventually, concentrations return to values dictated by equilibrium of ambient waters with fluorite (typically in the 4 to 8 ppm range).

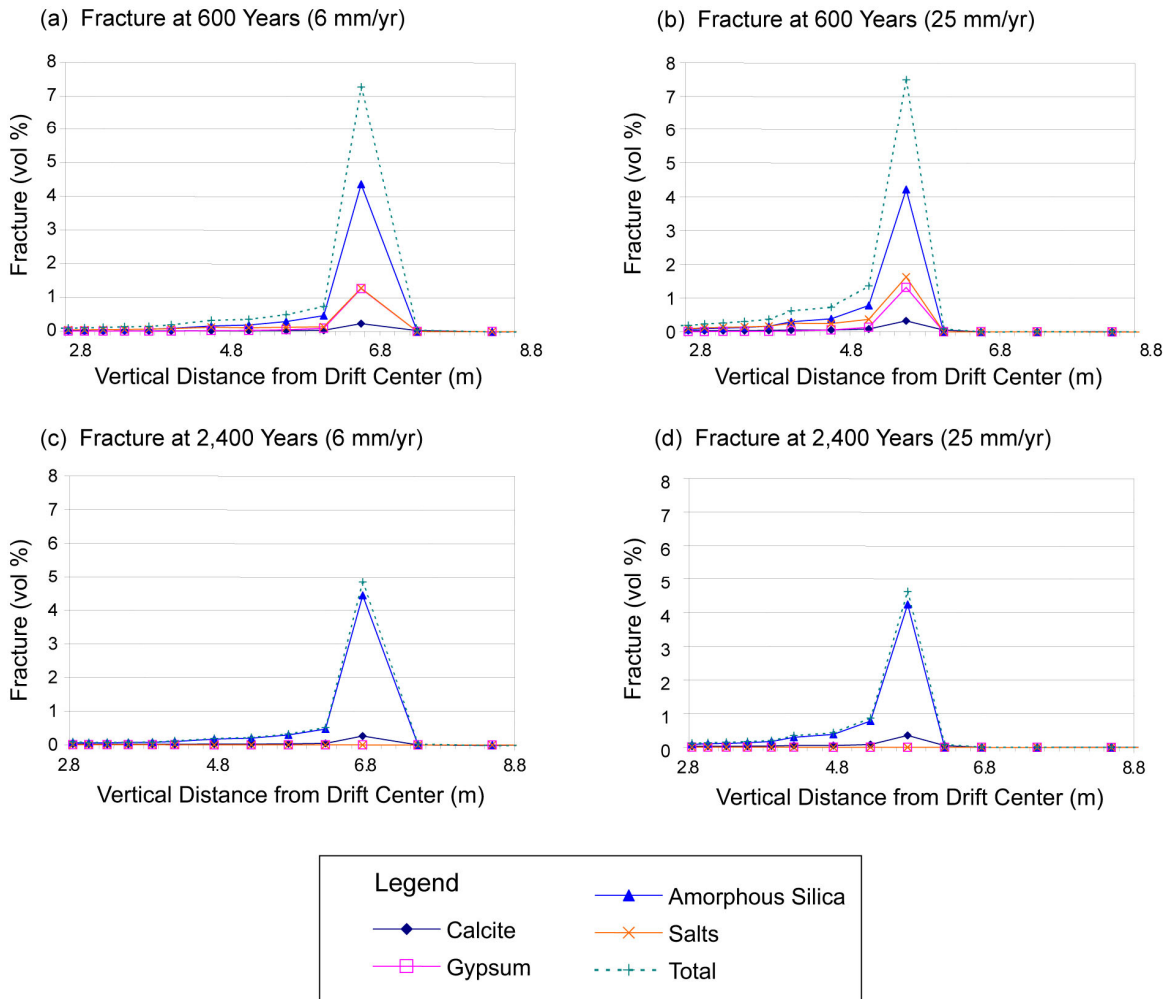
F.4.3 Mineral Alteration, Porosity and Permeability Changes, and Evaporitic Precipitation

The results of thermal-hydrologic simulation without considering evaporitic precipitation and any chemical reactions demonstrate the capillary barrier effect of the drift; which works to deflect ambient water percolation and condensate around the drift. Taking a data point far enough away from the drift as a reference for ambient saturation value, liquid saturations in fractures above the drift crown are found to be relatively increased but significantly decreased below the drift (shadow zone), at 2,400 years, a time well after the end of the boiling phase (BSC 2003a, Section 6.8.5.4, Figure 6.8-39).

Soluble chloride, nitrate salts, and minerals precipitate in the dryout zone and its periphery area because of evaporation and chemical reactions. The presence of these new precipitates leads to a change of porosity and a modification of permeability. The fracture permeability changes are approximated by a cubic law relation through the hydraulic aperture adjustment to mineral precipitation or dissolution. The initial hydraulic aperture of fractures is determined from fracture spacing and permeability (ascertained by air-permeability measurements) (BSC 2003a, Section 6.4.4.2). And matrix permeability changes are calculated from changes in porosity due to precipitation or dissolution (BSC 2003a, Section 6.4.4.3).

THC simulation with water W0 (Figure F-2a) shows that after the same simulated time period as for the thermal-hydrologic model, a zone of higher liquid saturation has formed 7 to 8 m above the drift, reflecting partial diversion of flow at this location. This flow diversion effect results from a thin region of significantly lower permeability (Figure F-2b) created by prior mineral deposition at the boiling front. In this case, the permeability has decreased by a factor of about 10 in this area. Correspondingly, the shadow zone extends somewhat deeper below the drift, and liquid saturations at the drift crown are somewhat reduced, compared to the thermal-hydrologic simulation results. Results using water W5 as initial composition show a more pronounced flow diversion effect (BSC 2003a, Figure 6.8-41a), with the permeability decreasing by two to three orders of magnitude (BSC 2003a, Figure 6.8-41b) in the thin region of mineral precipitation. The results using the other waters are very similar. Consequently, the shadow zone below the drift is extended significantly when considering chemical effects.

The permeability decrease results primarily from the precipitation of amorphous silica and, to a lesser extent, calcite (BSC 2003a, Figures 6.8-43 to 6.8-46). Various waters (W0 to W7) induce similar mineral changes, and Figure F-9 shows the mineral change for W0 water. The fracture porosity is predicted to decrease by approximately 4% to 7%. The maximum porosity decrease occurs in a thin zone during refluxing at the edge of the dryout zone, before the dissipation of this zone around the drift. By 2,400 years (with the simulations employing vapor-pressure lowering), fractures have rewetted, and the amount of precipitated solids (BSC 2003a, Figure 6.8-46) remains essentially unchanged for the remainder of the entire simulated time period.



Source: BSC 2003a, Figure 6.8-44.

NOTE: Profiles are shown for simulated times of 600 and 2,400 years for simulations using water W0 with vapor-pressure lowering and two different fixed infiltration rates (6 and 25 mm/yr).

Figure F-9. Vertical Profile of Simulated Mineral Abundances above the Drift Crown

Model results show that illite and stellerite are the most significant minerals precipitating in the rock matrix, with maximum amounts around 1% of the matrix porosity (BSC 2003a,

Section 6.8.5.4). The modification of permeability in the rock matrix because of mineral precipitation is smaller than that of fractures.

F.4.4 Thermal-Hydrologic-Chemical Model Validation

The model validation of Revision 2 of *Drift-Scale Coupled Processes (DST and THC Seepage) Models* (BSC 2003a) includes simulations and comparisons with the results of the in situ Drift Scale Test, the indoor laboratory plug-flow reactor experiment, and fracture sealing experiment. The Drift Scale Test was simulated in the THC model in Revision 1 of the report (BSC 2002a) but did not appear in the validation section. The plug-flow reactor experiment was the only test included in the validation study in Revision 1 (BSC 2002a, Sections 6.2 and 6.7). The Drift Scale Test is an in situ heater test. The purpose of the test was to evaluate the coupled thermal, hydrologic, chemical, and mechanical processes that take place in unsaturated fractured tuff over a range of temperatures (approximately 25°C to 200°C). Details of the Drift Scale Test are discussed in *Thermal Testing Measurements Report* (BSC 2002b, Section 6.3) and in the *Drift Scale Test As-Built Report* (CRWMS M&O 1998). The plug-flow reactor experiment investigated tuff dissolution and precipitation under isothermal elevated temperature conditions (BSC 2003a, Section 7.2), where the fracture sealing experiment is a condensate fluxing experiment in a fracture network under a boiling environment (BSC 2003a, Section 7.3). The observation data from these tests have been used to validate the THC models. All the simulations for these tests met their respective validation criteria (BSC 2003a, Sections 7.1.7, 7.2.1, and 7.3.1).

F.4.4.1 Drift Scale Test and Model

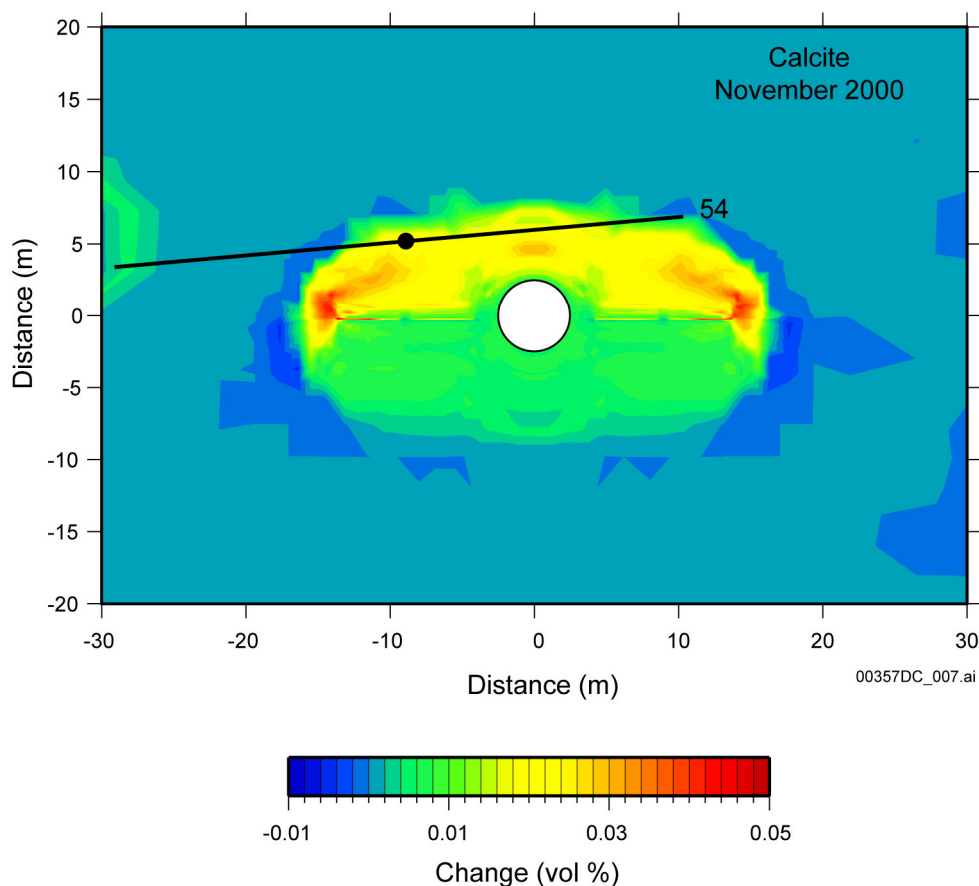
The Drift Scale Test and the observation data collected from the test provide the primary means of validation for the drift-scale THC seepage model. The geochemical measurements were performed on gas, water, and mineral samples collected from the full 4-year heating phase of the Drift Scale Test. The Drift Scale Test THC model and model validation of simulation results against measurements are presented in *Drift-Scale Coupled Processes (DST and THC Seepage) Models* (BSC 2003a, Section 7.1).

The Drift Scale Test is located in Alcove 5 of the Tptpmn geologic unit in the Exploratory Studies Facility. The alcove is a drift approximately 50 m long and 5 m in diameter, in which nine electrical floor canister heaters were placed to simulate nuclear-waste-bearing containers. Electrical heaters were also placed in a series of horizontal boreholes (wing heaters) drilled perpendicularly outward from the central axis of the drift. The Drift Scale Test was planned for a period of 4 years of heating, followed by 4 years of cooling. The Drift Scale Test heaters were activated on December 3, 1997, and were switched off on January 14, 2002. Since then, the test area has been slowly cooling.

The strong thermal load, which simulated the heat load of a waste package applied to the system, is the driving force for changes in the hydrologic and chemical behavior of the system. The resulting changes in temperature, liquid saturation, and gas-phase composition lead to changes in the chemistry of water and gas, as well as mineral dissolution and precipitation. The THC model validation against the Drift Scale Test, including the thermal and hydrologic evolution, gas-phase

CO₂ evolution, aqueous species evolution, mineralogical changes, and porosity and permeability is discussed (BSC 2003a, Sections 7.1.9 to 7.1.13).

Calcite, amorphous silica, and a calcium sulfate phase (gypsum) are the only phases identified so far as products of the processes taking place during the Drift Scale Test. Amorphous silica appears as glassy coatings covering larger areas of the surface, commonly in the form of thin curled sheets and fine tubules. Calcite typically is found as scattered, small, late-stage mounds, with gypsum as very late-formed scattered crystals on top of other phases. The percentage of mineral precipitates in the fracture system could not be determined from this type of localized analysis. Some of the silica coatings were approximately 10 to 20 μm thick, with discrete gypsum crystals up to 80 μm long. Given a uniform 10- μm -thick layer of mineral precipitates on one side of the fractures, with a hypothetical range in fracture apertures of 100 to 1,000 μm , the proportion of fracture volume filled would range from 1% to 10%. Because many of the coatings are much less than 10 μm thick and do not cover all areas of every fracture, the volume filled is likely to be less than 1%. Amorphous silica was the dominant phase precipitated during boiling, with much smaller amounts of calcite and gypsum. Figure F-10 shows the modeled calcite distribution changes and the locations of observed calcite in the Drift Scale Test. The calcite abundances in the precipitation zone above the heaters are increased relative to ambient conditions. Calcite dissolution appears to be minor. The location of modeled calcite precipitation matches the location of observed calcite in the sidewall core sample (BSC 2003a, Section 7.1.12). Precipitations of amorphous silica and gypsum show similar results with the calcite in the simulations (BSC 2003a, Section 7.1.12, Figures 7.1-38, 7.1-39).



Source: BSC 2003a, Figure 7.1-37.

NOTE: Chemistry borehole 54 is shown, with the location of observed calcite (the filled circle) formed during Drift Scale Test.

Figure F-10. Modeled Volume Percent Change in Calcite in Fractures as of November 2000 (35 Months of Heating)

The validation of the THC models by comparison to chemical data on water and gas samples is subject to a variety of uncertainties because of the wide ranges that parameters can take (BSC 2003a, Section 7). First, thermal-hydrologic processes can cause large differences in the chemistry of water and gases over very small increments in temperature as a result of boiling and mineral-water reactions (BSC 2003a, Section 7.1.10.2). In contrast, temperature exhibits much less variation in space, because it is governed mainly by conduction in the rock matrix. Second, large differences in aqueous species concentrations that develop in pore water in fractures and the adjacent matrix can be maintained because of the slow rates of diffusion of aqueous species (BSC 2003a, Section 7.1.11.3). Third, changes that the samples undergo during their extraction from the rock (e.g., cooling, degassing, condensation) have the potential for shifting the aqueous species compositions by a few orders of magnitude.

The uncertainty of the model is discussed in *Drift-Scale Coupled Processes (DST and THC Seepage) Models* (BSC 2003a, Table 6.9-1, Sections 6.9.1 and 6.9.2). The uncertainties

associated with the THC model are quantified in several ways. Variation of input water compositions is represented by five types of input waters (BSC 2003a, Section 6.2.2.1). The effect of future climate changes is considered by variations in infiltration rates (BSC 2003a, Section 6.8.2, Table 6.8-2). The subsequent uncertainty in gas diffusion is studied by varying the CO₂ effective diffusivity (BSC 2003a, Section 6.8). Finally, the effect of vapor-pressure lowering (caused by capillary pressure) is also incorporated (BSC 2003a, Sections 6.8.5.2, 6.8.5.3).

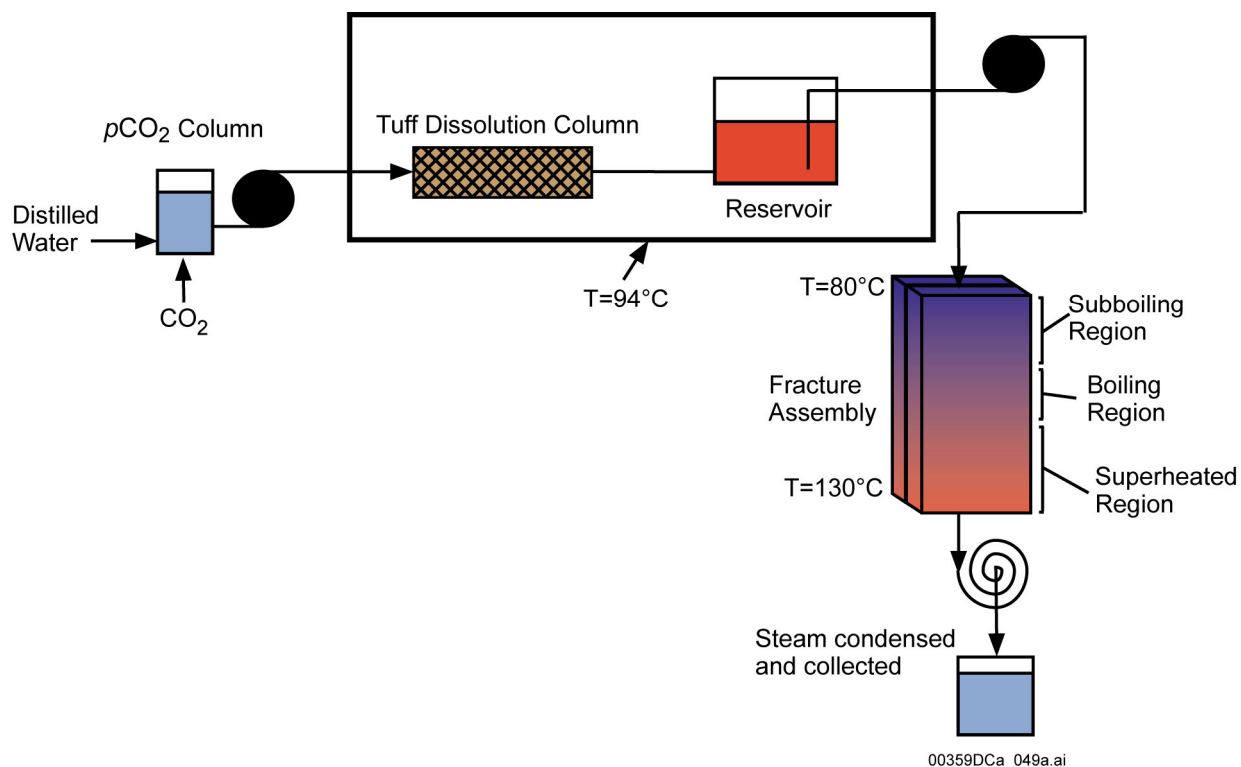
The main impact of vapor-pressure lowering is seen in the smaller extent of dryout around the drift in the rock matrix than in fractures, even though temperatures are essentially the same in both media (BSC 2003a, Figure 6.8-6; also compare with Figure 6.7-4). Consequently, the rock matrix at the drift wall rewets earlier (at around 200 to 300 years) than in previous models (1,200 to 1,400 years) (BSC 2003a, Figure 6.8-8). In fractures, however, the time of rewetting around the drift wall is similar for both model revisions (Figure 6.8-7) (BSC 2003a, Sections 6.8.5.2)

F.4.4.2 Plug-Flow Reactor Experiment

The setup of the tuff dissolution experiment, along with the fracture sealing experiment discussed below, is shown in Figure F-11. The experiments were performed under elevated temperatures to simulate thermal effect from the waste emplacement heat loading. In the experiment, boiling, evaporation, and condensation processes in the rock matrix and fractures were effectively replicated to capture the THC effects on Yucca Mountain fractured tuffs.

The plug-flow reactor experiment was a column experiment used to test the dissolution and precipitation in Yucca Mountain tuffs under elevated temperature (BSC 2003a, Section 7.2). Its purpose was to test geochemical models that were developed for the Drift Scale Test THC and the Tptpmn and Tptpll THC seepage models. The observation data from the test was used to evaluate the sensitivity of the geochemical models to the mineral surface area, rock composition, mineral thermodynamic data, and changes to the TOUGHREACT code. Measured water compositions of samples obtained during the duration of the experiment also allowed the evaluation of kinetically controlled reactions with time.

For the tuff dissolution experiment, overcores of Topopah Spring tuffs (Tptpmn) from a borehole in the Exploratory Studies Facility were crushed, sieved, and washed. The crushed tuff was packed into a 29.8 cm long by 7.5 cm diameter polypropylene tube. The experiment was performed under isothermal conditions at elevated temperatures.



Source: BSC 2003a, Figure 7.2-1.

Figure F-11. Schematic Diagram of the Tuff Plug-Flow and Fracture Sealing Experiments

The inlet fluid consisted of deionized water initially equilibrated with a CO_2/N_2 gas mixture of 50,200 ppm CO_2 at 17°C . The resulting water had a measured pH of 4.58. This water was heated to 94°C and then introduced into the tuff column (also at 94°C) at a rate of 25 mL/hr. Water exiting the tuff column was collected in a reservoir and sampled periodically for chemical analysis over the length of the experiment (63.8 days).

A series of isothermal one-dimensional TOUGHREACT simulations was performed to model tuff dissolution (BSC 2003a, Section 7.2), using a 149-element mesh, with dimensions and grain size identical to those of the plug-flow experiment, plus one additional boundary element to obtain the appropriate outlet conditions. The results of these simulations and the experimental data are shown in *Drift-Scale Coupled Processes (DST and THC Seepage) Models* (BSC 2003a, Figure 7.2-3). The measured concentrations of the dissolved components initially increased rapidly and then declined until about 11 days, after which relatively steady concentrations were achieved (BSC 2003a, Figure 7.2-3). The high initial measured concentrations may have resulted from the dissolution of fine tuff particles not removed in the washing process, which resulted in a much higher available reactive surface area at the start of the experiment, or from the initial mineral surfaces being more reactive because of crushing and surface roughness, none of which is accounted for in the simulations. Dissolution is sensitive to the value of surface area used in the simulations because surface area affects the kinetic mineral reactions controlling the concentrations of the modeled species in solution. There is a close match between the measured and calculated concentrations of Na^+ and $\text{SiO}_2(\text{aq})$ for the 60 μm grain-size (BSC 2003a, Section 7.2.2, Tables 7.2-2, 7.2-3) (larger surface area/unit volume than that of 120 μm) simulation.

The simulations of the tuff dissolution experiments met the criterion for model validation, which is that the modeled concentrations for the major dissolved species (mg/L) in the effluent should be within one order of magnitude of the measured average steady-state concentrations (BSC 2003a, Section 7.2.1). The simulations are sensitive to a number of parameters, including the initial mineral assemblage and the mineral surface area. Discussion of uncertainty associated with coupled process (THC) modeling is presented in *Drift-Scale Coupled Processes (DST and THC Seepage) Models* (BSC 2003a, Section 6.9).

F.4.4.3 Fracture Sealing Experiment

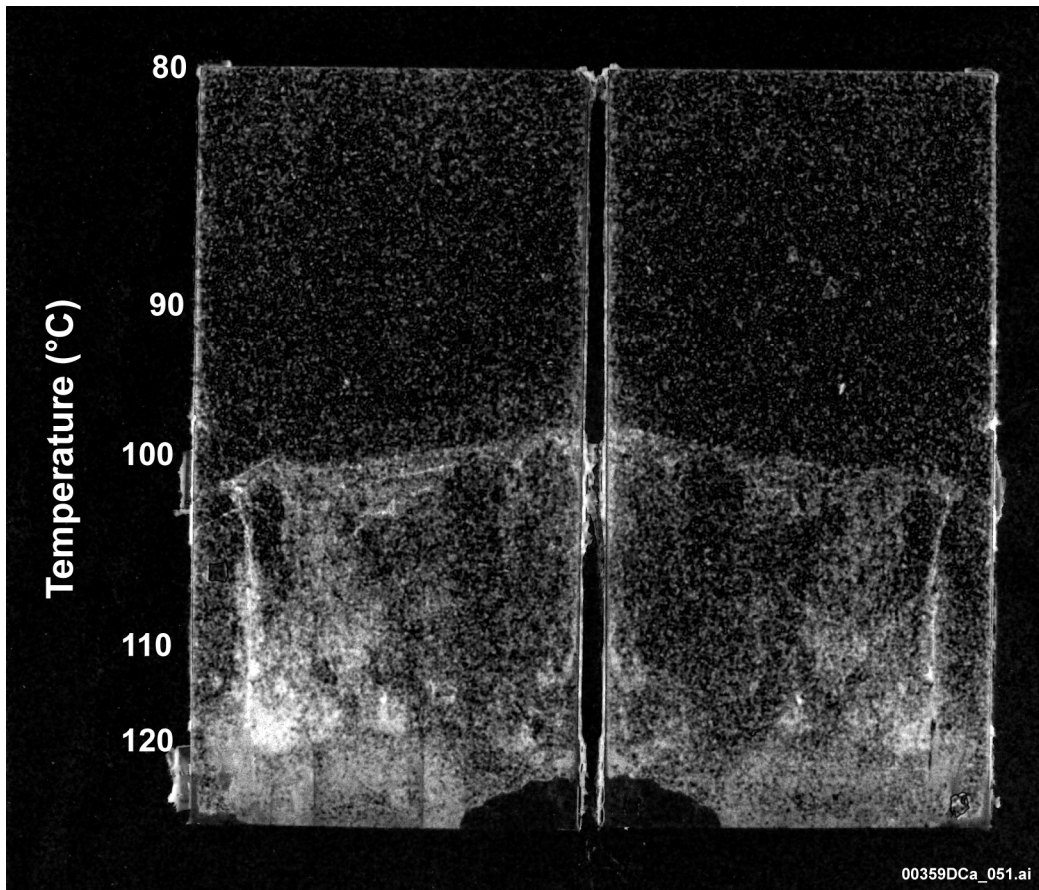
The fracture sealing experiment measured the effects of the condensate flux under boiling conditions in a fracture (Figure F-11). Two saw-cut blocks of welded rhyolite ash-flow tuff, measuring 31.7 cm tall, 16.2 cm wide, and 3.2 cm thick, were separated by 17.7 μm gold shims to create a vertical planar fracture. The blocks, taken from the Tptpmn of the Exploratory Studies Facility, contained a small fracture that intersected the saw-cut but did not have any visible lithophysal cavities. The mineralogy of the tuff samples is similar to the samples used for the tuff dissolution experiment because they are from the same Tptpmn layer (BSC 2003a, Section 7.3).

The outer surfaces of the blocks were sealed with Dow Corning 1199 silicone, and the vertical sides of the fracture were sealed with an aluminum sheet coated with silicone. Polypropylene endcaps were secured to the assembly with stainless steel bands, with ports at the top and bottom to allow for the introduction of fluid at the top and collection of vapor at the base.

Heating was applied through the use of electrical resistance heaters mounted directly on the sides of the blocks. A vertical temperature gradient was established within the block assembly, with a temperature of 80°C at the top and 130°C at the bottom. Temperatures were monitored throughout the experiment with a series of thermocouples located at 2.7, 7.1, 11.5, 15.9, 20.3, 24.7, and 29.1 cm from the base of the blocks and 0.6 cm from the fracture surface along the centerline of the block.

After steady-state chemical conditions were attained in the plug-flow reactor, a portion of the water generated from the reactor was flowed at a rate of 10.8 mL/hr into the top of the fracture. After 5 days, the fracture began to seal, as evidenced by a declining outflow rate, leaks in the inlet side of the fracture, and the need for increased pressure to maintain a constant inlet flow rate. After several unsuccessful attempts to plug leaks and the near-zero rate of effluent (condensate from vapor) collection, it was concluded that the aperture was effectively sealed.

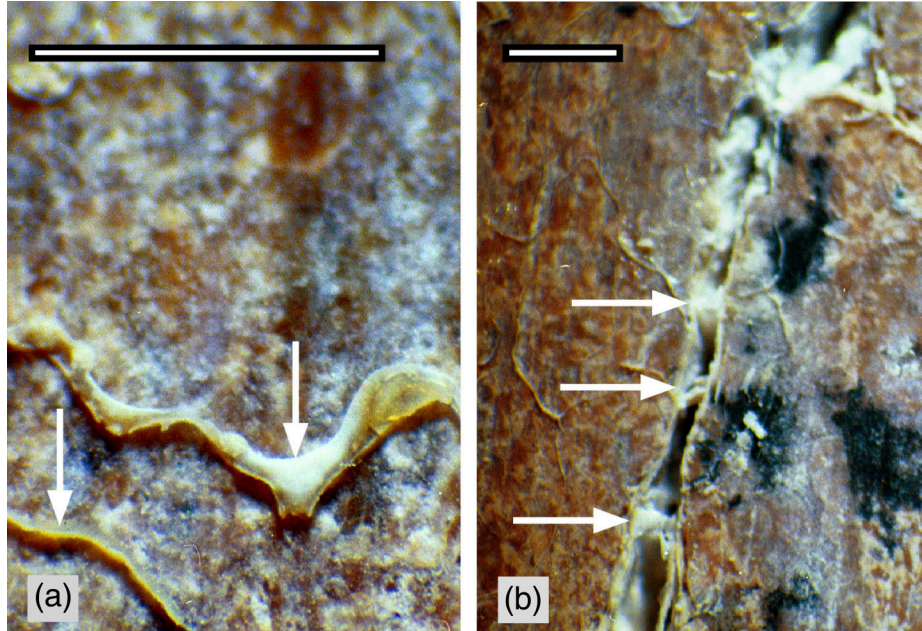
After cooling, the fracture was opened and examined to determine the location and nature of secondary mineral formation. The precipitate (identified as mainly amorphous silica from scanning electronic microscope (SEM), X-ray analyses and visual and petrographic examination) was deposited almost exclusively at locations where temperatures exceeded 100°C (Figure F-12). Bridging structures of amorphous silica that formed during the experiment in both the saw-cut fracture and the natural fracture (Figure F-13) appear to have obstructed fluid flow within the fracture system. Secondary opal-A deposited as “mounds” on fracture and borehole surfaces were noted at the Single Heater Test site (CRWMS M&O 1999, Sections 6.4.3.1 and 6.4.5).



Source: BSC 2003a, Figure 7.3-1.

NOTE: An enhanced image shows fracture temperature profile and fluorescing precipitate (light shades) under ultraviolet illumination on both fracture faces. Vertical dimension is 0.317 m.

Figure F-12. Opened Fracture Faces at Conclusion of Fracture Sealing Experiment



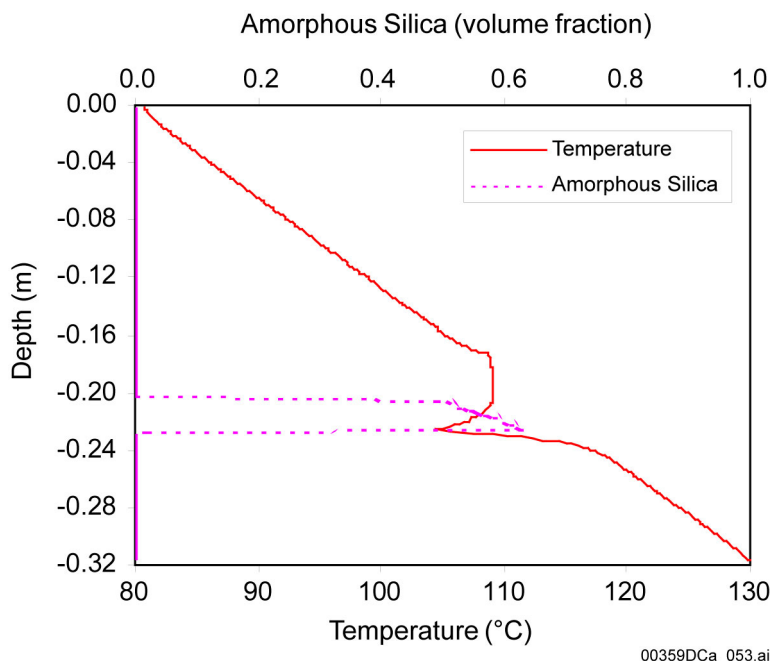
00359DCa_052.ai

Source: BSC 2003a, Figure 7.3-2.

NOTE: Scale bars are 0.5 mm.

Figure F-13. Bridging Structures (Identified with Arrows) (a) Extending Outward from Flat Fracture Face; (b) Spanning Aperture in Cross-Cutting Natural Fracture

Fracture sealing was observed after 5 days, occurring after only a relatively small fraction (1.2% to 4.7%) of the total fracture porosity filled with solid precipitate (consisting primarily of amorphous silica) (BSC 2003a, Section 7.3). The simulation results indicated the formation of a nearly isothermal two-phase region (Figure F-14), with an overlying water column above and a vapor zone below (Figure F-11). The precipitation of amorphous silica at the base of the two-phase zone accounted for the porosity and permeability reduction in the fracture system. A gradual pressure buildup, caused by the silica precipitation and resultant reduction of the fracture aperture, occurred at the top of the fracture system. The experimental system experienced a similar phenomena, as reduced permeability led to the need for higher inlet pressure to sustain a constant injection rate, resulting in fluid leaking out along the sides and top of the fracture system (BSC 2003a, Section 7.3.2).



Source: BSC 2003a, Figure 7.3-4.

NOTE: Simulation has amorphous silica controlled by kinetic precipitation and dissolution.

Figure F-14. Simulated Temperature Profile and Volume Fraction of Amorphous Silica versus Depth at 5.01 Days

In summary, significant permeability reductions because of fracture sealing occurred within 5 days after initiation of fluid flow in both the experiment and the simulations. This is related to the observation that silica precipitation throughout the boiling zone in the experimental fracture system occurs at early time. This silica-precipitating phenomenon is better simulated with a kinetic approach rather than an equilibrium approach (BSC 2003a, Figures 7.3-3a and 7.3-3b). The simulation results met the qualitative validation criteria. These simulations capture the two main observed results of the experiments: the location of the precipitate, and its mineralogy (BSC 2003a, Section 7.3.1).

F.4.5 CHn Hydrogeologic Units

This section is the basis for the response to KTI ENFE 1.03 AIN-1 regarding the coupled THC alterations of the CHn unit. The conclusion is made from the simulation results regarding porosity, permeability, and mineralogical changes.

In Revision 2 of *Drift-Scale Coupled Processes (DST and THC Seepage) Models* (BSC 2003a), the model domain has been extended beyond the CHn unit to the groundwater table, to capture the temperature rise in the CHn. The heat capacity, and thermal conductivity of the CHn unit and other units in the model domain were estimated using field measurements (BSC 2003a, Section 4.1.1, Table 4.1-1).

In the mountain-scale TH model, the heating at the repository achieves the strongest thermal effect from 500 to 1,000 years. After 1,000 years, the thermal effect starts decreasing. After

2,000 years, the temperatures at and near the repository are significantly cooled down. At 5,000 years, the majority of the system returns almost to ambient conditions, with temperatures at the remaining hottest spots within the repository area only 60°C or less (BSC 2003b, Section 6.3.1.1, Figures 6.3.1-5a and 6.3.1-5b). The spatial distribution of temperature around the drift at 600 years is shown in Figure F-1.

In comparison, the thermal pulse from the repository heat load reaches its peak later at the top of the CHn unit. The temperature along the top of the CHn unit increases from its ambient 27°C to above 50°C at 500 years, to 65°C at 1,000 years, and to 75°C at 2,000 years, respectively (BSC 2003b, Figures 6.3.1-2c, 6.3.1-3c, and 6.3.1-4c). The time for far-field temperatures to reach their peak values is about 2,000 years after waste emplacement. The temperature increase throughout the whole CHn unit is expected to be smaller than that at the top of the CHn unit. The modification of CHn hydraulic properties was considered through porosity and resultant permeability changes resulting from the THC effect.

The fracture permeability change is sensitive to porosity change. In the drift-scale THC simulations, using effective (hydraulic) apertures, a 10% to 14% drop in fracture porosity leads to zero permeability in fractures in the modeled repository unit (BSC 2003a, Section 6.4.6.1). However, the validation study of the THC simulation of the Drift Scale Test shows that the volume of fractures filled is likely to be less than 1% (BSC 2003a, Sections 7.1.12). This suggests that thermal modification of hydrologic properties of the fractures in the CHn unit, where lower temperatures are predicted, is expected to be small.

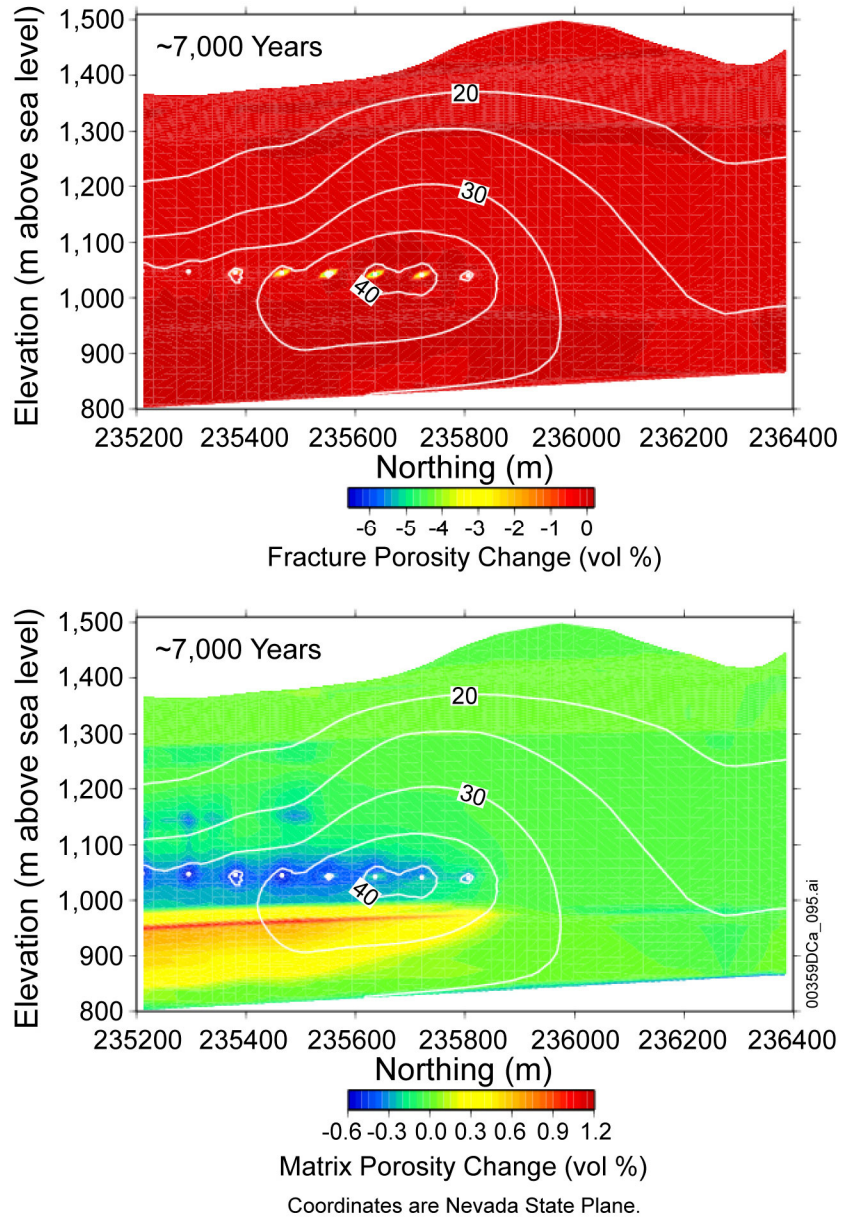
The thermal properties of the CHn unit can be altered in two ways: by addition of new minerals resulting from precipitation, and mineral composition and structural change under long-term (many years of) heating. In the THC models, the thermal properties of modeled layers are not directly modified to account for precipitated minerals (BSC 2003a, Section 6.4.6.1, approximation 2). This is based on findings that the mass of minerals precipitated is small and the alteration of thermal properties in the rocks is considered insignificant.

Heating may alter the clay minerals in the CHn unit, which may affect hydrologic and thermal properties. The non-welded tuff in the CHn unit in the northern part of the mountain-scale model domain has variably-altered clay minerals (zeolites) (BSC 2003f, Sections 5.2, 6.6.3, Figure 5, and Table 11). Zeolites are a group of hydrated aluminosilicate minerals corresponding chemically to feldspars plus water plus or minus silica (Drever 1997, Glossary of Geological Terms). Some zeolites have significant cation-exchange capacities (Drever 1997, Glossary of Geological Terms); the zeolitic layers are consequently viewed as an important barrier to radionuclide migration. The possible changes of clay-mineral thermal properties under heating are not known. The major concerns include potential loss of structural water and irreversible structural change under long-term thermal influences, leading to possible changes in porosity and permeability, and modification of sorption properties.

The vitric and zeolitic tuffs in the CHn unit undergo some degree of alteration under thermal conditions. The mountain-scale THC modeling qualitatively indicates that at temperatures above approximately 50°C, the CHn unit would undergo potential alterations of vitric tuffs and zeolite; however, changes in porosity and permeability are insignificant. Volcanic glass and/or zeolites in the vitric and zeolitic tuffs in the CHn unit would likely undergo alteration at elevated

temperatures. Model results show that after 1,000 years, over 5% of the volcanic glass in the rock matrix of the TSw basal vitrophyre (at the bottom of the TSw unit and over the top of the CHn unit) has reacted and altered, and by 7,000 years it has dissolved up to nearly 20% in volume (BSC 2003b, Figure 6.4-20). The zone of alteration extends down into the CHn unit as temperatures increase. Much of the reaction has taken place by 3,000 years, with the alteration rate decreasing strongly as temperatures decline in the rocks below the repository. Additionally, in the CHn zeolitic tuffs below the repository, calcite minerals are dissolved in 1,000 to 2,000 years where there are increasing CO₂ concentrations and decreasing pH (BSC 2003b, Section 6.4.3.3.3).

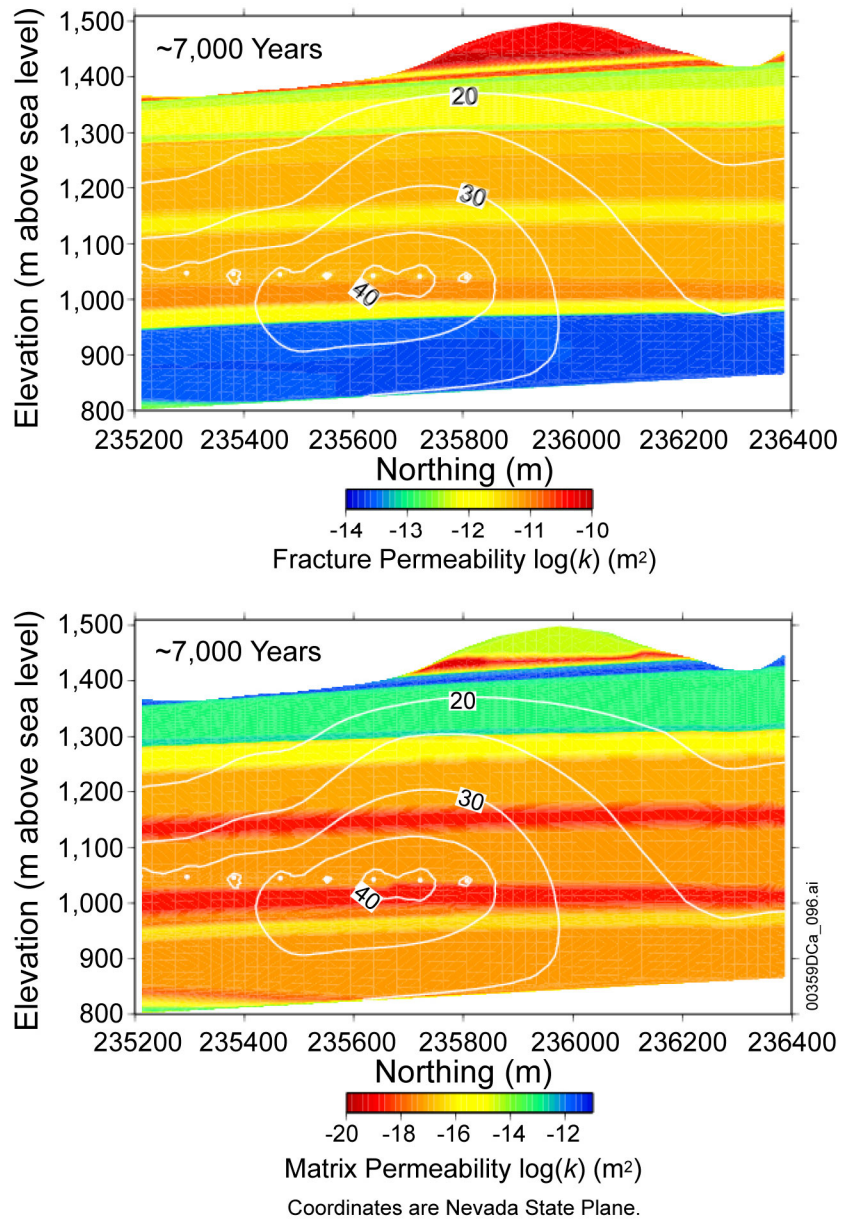
Consequently, hydrologic properties of the CHn unit are slightly modified. There is a modest increase in matrix porosity of about 1% (Figure F-15), primarily owing to the reaction of clinoptilolite and glass to feldspars and stellerite. In contrast, in the repository horizon around the drifts, there is a small reduction in rock matrix porosity (less than 0.6%). The porosity changes result from the net effect of pore volume adjustments to mineral precipitation and dissolution. The fracture and matrix permeability values estimated using the altered porosity values after 7,000 years are shown in Figure F-16. The changes in rock matrix permeability of the CHn vitric and zeolitic units are considered to be minor because of the initially high porosity (approximately 27% to 35%) of these rock layers (BSC 2003g, Tables 3 and 6). In Figure F-16, fracture permeability is generally three orders of magnitude larger than matrix permeability. Given the importance of fractures in unsaturated water flow, the 1% increase in matrix porosity would increase matrix permeability; however, relative to fracture permeability, this increase would be insignificant. These simulation results demonstrate that there is no appreciable change in fracture permeability in the CHn layer after 7,000 years (Figure F-16). Therefore, the simulation demonstrates that the porosity and permeability values after 7,000 years are essentially the same as the initial values (BSC 2003b, Section 6.4.3.3.4).



Source: BSC 2003b, Figure 6.4-25.

NOTE: The cross section is a north-south vertical profile transecting eight repository drifts of the northern part of the repository and its neighboring nonrepository region (BSC 2003b, Figures 6.4-2 and 6.4-3). The eight small spots at elevation of about 1,050 m are locations of the repository drifts.

Figure F-15. Fracture and Matrix Porosity Changes after 7,000 Years from the Mountain-Scale Thermal-Hydrologic-Chemical Model



Source: BSC 2003b, Figure 6.4-26.

NOTE: The cross section is a north-south vertical profile transecting eight repository drifts of the northern part of the repository and its neighboring nonrepository region (BSC 2003b, Figures 6.4-2 and 6.4-3). The eight small spots at elevation of about 1,050 m are locations of the repository drifts.

Figure F-16. Fracture and Matrix Permeability after 7,000 Years from the Mountain-Scale Thermal-Hydrologic-Chemical Model

The extent of glass alteration is limited to the strongly heated regions directly below the repository drifts (BSC 2003b, Section 6.4.3.3.3). The effect of THC processes on the porosity and permeability is considered to be limited to at or near the drifts, and mountain-scale flow as a whole is not significantly affected.

The above mountain-scale THC modeling results concerning the alteration of the vitric tuffs and zeolite in the CHn unit are considered to be qualitative because there are uncertainties in the compositional, thermodynamic, and kinetic data representing relevant mineral-water reactions (BSC 2003b, Section 6.4.3.3.3). More rigorous analysis of clay mineral phase changes under continued heating would provide more insight into changes in hydrologic and thermal properties within the CHn unit. However, mountain-scale THC modeling results qualitatively indicate that possible phase changes incurred by heating are expected to be insignificant because the temperature rise at the CHn unit from waste emplacement heat loading is small.

In summary, thermal effects on the hydrologic properties of the CHn unit are expected to be relatively small because this unit is quite far away from the drift. The temperature rise in the CHn unit is simulated to be smaller than that at the repository horizon. The thermal effect on the hydrologic properties of the CHn unit is incorporated within the THC modeling through the modification of porosity and permeability. Based on the observation that only a small amount of minerals precipitated in the Drift Scale Test, the thermal properties of the CHn unit are not modified for thermal effects in the THC simulation. Generally speaking, the thermal effects on the CHn unit are appropriately addressed in the simulations with the current available knowledge. Results from the mountain-scale THC model indicate that possible phase changes of the vitric tuffs and zeolite clay minerals within the CHn unit under waste emplacement heat loading are inconsequential because of the minimal temperature rise.

F.5 REFERENCES

BSC (Bechtel SAIC Company) 2002a. *Drift-Scale Coupled Processes (DST and THC Seepage) Models*. MDL-NBS-HS-000001 REV 01 ICN 02. Las Vegas, Nevada: Bechtel SAIC Company. ACC: MOL.20020312.0156.

BSC 2002b. *Thermal Testing Measurements Report*. ANL-NBS-HS-000041 REV 00. Las Vegas, Nevada: Bechtel SAIC Company. ACC: MOL.20021004.0314.

BSC 2003a. *Drift-Scale Coupled Processes (DST and THC Seepage) Models*. MDL-NBS-HS-000001 REV 02. Las Vegas, Nevada: Bechtel SAIC Company. ACC: DOC.20030804.0004.

BSC 2003b. *Mountain-Scale Coupled Processes (TH/THC/THM)*. MDL-NBS-HS-000007 REV 01. Las Vegas, Nevada: Bechtel SAIC Company. ACC: DOC.20031216.0003.

BSC 2003c. *Abstraction of Drift-Scale Coupled Processes*. MDL-NBS-HS-000018 REV 00. Las Vegas, Nevada: Bechtel SAIC Company. ACC: DOC.20031223.0004.

BSC 2003d. *In-Drift Precipitates/Salts Model*. ANL-EBS-MD-000045 REV 01 ICN 01B. Las Vegas, Nevada: Bechtel SAIC Company. ACC: DOC.20031028.0003.

BSC 2003e. *UZ Flow Models and Submodels*. MDL-NBS-HS-000006 REV 01. Las Vegas, Nevada: Bechtel SAIC Company. ACC: DOC.20030818.0002.

BSC 2003f. *Development of Numerical Grids for UZ Flow and Transport Modeling*. ANL-NBS-HS-000015 REV 01. Las Vegas, Nevada: Bechtel SAIC Company. ACC: DOC.20030404.0005.

- BSC 2003g. *Calibrated Properties Model*. MDL-NBS-HS 000003 REV 01. Las Vegas, Nevada: Bechtel SAIC Company. ACC: DOC.20030219.0001.
- BSC 2004. *Engineered Barrier System: Physical and Chemical Environment Model*. ANL-EBS-MD-000033 REV 02. Las Vegas, Nevada: Bechtel SAIC Company. ACC: DOC.20040212.0004.
- CRWMS M&O (Civilian Radioactive Waste Management System Management and Operating Contractor) 1998. *Drift Scale Test As-Built Report*. BAB000000-01717-5700-00003 REV 01. Las Vegas, Nevada: CRWMS M&O. ACC: MOL.19990107.0223.
- CRWMS M&O 1999. *Single Heater Test Final Report*. BAB000000-01717-5700-00005 REV 00 ICN 1. Las Vegas, Nevada: CRWMS M&O. ACC: MOL.20000103.0634.
- CRWMS M&O 2000. *Drift-Scale Coupled Processes (DST and THC Seepage) Models*. MDL-NBS-HS-000001 REV 00. Las Vegas, Nevada: CRWMS M&O. ACC: MOL.19990721.0523.
- CRWMS M&O 2001. *Drift-Scale Coupled Processes (DST and THC Seepage) Models*. MDL-NBS-HS-000001 REV 01. Las Vegas, Nevada: CRWMS M&O. ACC: MOL.20010314.0003.
- Drever, J.I. 1997. *The Geochemistry of Natural Waters, Surface and Groundwater Environments*. 3rd Edition. Upper Saddle River, New Jersey: Prentice Hall. TIC: 246732.
- Gascoyne, M. 2003. "Soluble Salts in the Yucca Mountain Tuff and their Significance." *Proceedings of the 10th International High-Level Radioactive Waste Management Conference (IHLRWM), March 30-April 2, 2003, Las Vegas, Nevada*. Pages 340–347. La Grange Park, Illinois: American Nuclear Society. TIC: 254202.
- Lu, G.; Sonnenthal, E.L.; and Bodvarsson, G.S. 2003. "Implications of Halide Leaching on ³⁶Cl Studies at Yucca Mountain, Nevada." *Water Resources Research*, 39 (12), 3/1–3/15. Washington, D.C.: American Geophysical Union. TIC: 255498.
- Pruess, K.; Oldenburg, C.; and Moridis, G. 1999. *TOUGH2 User's Guide, Version 2.0*. LBNL-43134. Berkeley, California: Lawrence Berkeley National Laboratory. TIC: 253038.
- Reamer, C.W. 2001. "U.S. Nuclear Regulatory Commission/U.S. Department of Energy Technical Exchange and Management Meeting on Evolution of the Near-Field Environment (January 9 - 12, 2001)." Letter from C.W. Reamer (NRC) to S. Brocoum (DOE/YMSCO), January 26, 2001, with enclosure. ACC: MOL.20010810.0033.
- Schlueter, J. 2002. "Evolution of the Near-Field Environment Key Technical Issue Agreements." Letter from J. Schlueter (NRC) to S. Brocoum (DOE/YMSCO), February 14, 2002, with enclosure. ACC: MOL.20020607.0086.
- Wu, Y.-S.; Pan, L.; Zhang, W.; and Bodvarsson, G.S. 2002. "Characterization of Flow and Transport Processes within the Unsaturated Zone of Yucca Mountain, Nevada, Under Current and Future Climates." *Journal of Contaminant Hydrology*, 54, (3–4), 215–247. New York, New York: Elsevier. TIC: 253316.